Dear Mrs Ali

Thank you for inviting us to revise our manuscript entitled “Triple oxygen and isotope systematics of evaporation and mixing processes in a dynamic desert lake system”. We are grateful to both you and the two reviewers for your detailed and constructive comments and suggestions. Please find attached a revised version of our contribution. A detailed point-by-point response to the reviewer’s comments was already provided in the individual author responses. Therefore, only the key issues unveiled by the reviewers are addressed below. A marked-up version of the revised manuscript is provided at the bottom of this file.

A major critical point concerned structural aspects. The revised version of the manuscript now follows a classical structure with separate Results and Discussion, which indeed improves the readability of the text, making key messages clearer. In detail, we have revised the introduction section to better point out the objectives of the manuscript. We have added a paragraph describing the Craig-Gordon model with major equations. Details on terminology and a table summarizing all variables used within the manuscript are now provided in the supplement. As suggested by both reviewers, we added a subsection on atmospheric vapour in the Methods section, where we now make clear why the OIPC model may not be suitable at our study site.

In the revised manuscript, we now discuss the possible isotope effect introduced by the freezing and thawing of our pan evaporation experiment. Additionally, we now include the results of laboratory experiments recently published by Gonfiantini et al. (2020) and compared them with our experimental data. These new findings greatly improve our understanding of the turbulence coefficient.

We have added a subsection on the isotopic residence times in ponds and lakes at the Salar del Huasco and extended our discussion on the model uncertainty to address the critique of one reviewer, who stated that we cannot infer information on the hydrological lake balance using isotope systematics. We show that combined triple oxygen and hydrogen isotope systematics do allow inferences on hydrological lake balance and fundamental hydrological processes.

Yours Sincerely

Claudia Voigt (on behalf of all co-authors)

Point-to-point response

Reply to Referee #1

The comments of reviewer #1 have contributed substantially to improving the paper. Please, find below in black the comments of the reviewer, in blue our responses to the comments and how these comments are addressed in the revised manuscript.

Firstly, the objectives and significance of the study are not clearly presented in the introduction. There is a limited introduction to the implication of using oxygen-17 other than "a potentially powerful tool" with much of the remaining introduction on oxygen-17 more suited to a methods section than an introduction. The importance of desert lake systems is central to this manuscript but is has limited emphasis only to oxygen-17. The objectives of the manuscript appeared to be only a sensitivity test of input variables in the Craig-Gordon model rather than assessing the dynamics of the salar system as a whole and using the Craig-Gordon model as a tool. The last part of the introduction seemed to be more of an abstract than an introduction and needs revision.

We thoroughly revised the introduction and focus now on hydrological processes that determine the isotopic composition of lakes and the larger implication of the ^{17}O-excess parameter as a tool to resolve these processes as well as to identify changes in the hydrological balance of lakes. We now stress the main objectives of the manuscript, which are: 1) test the potential of triple oxygen isotope analyses to resolve fundamental hydrologic processes of evaporation and mixing of sources that cannot be resolved by the classical δ^2H-δ^{18}O analyses; 2) test the robustness of the Craig-Gordon model in a highly dynamic environment with considerable seasonal variability in all the model input parameters; and 3) demonstrate the potential of triple oxygen isotope analyses to derive the hydrological balance of lakes from water isotope and climate monitoring.

Secondly, the issues with the presentation of the methods and sampling are closely related to the third issue (results and discussion). Some of the information in "Sampling" belongs in "Study Site" (e.g. connectivity of ponds) and the section would benefit from more emphasis on the different conditions of each area during the sampling periods. Through the "Sampling", "Methods", and "Craig-Gordon" sections (as well as some introduction parts) there are terms that are not introduced properly or defined (e.g. d-excess, E/I). The "Sampling" section does not include the measurement height of the atmospheric data that was collected (temperature, relative humidity, δv), which may be significant for use in the Craig-Gordon model. The section on Craig-Gordon modelling lacked sufficient detail to allow for the replicability of the results. The formulation of the Craig-Gordon model used for oxygen-17 was not provided (I assume it is a similar form to Surma et al., 2018) which would be useful for the readers to understand the sensitivity assessed by the authors. It would also be useful if the authors would provide the other values used in the Craig-Gordon model (e.g 17αl-v_evap, 17αl-v_diff). Additionally, there is no information on how the authors accounted for mixing. Is it changes to the input endmember? Is it changes to the E/I ratio?

We now address all of these points. In the revised manuscript we have now included a theoretical section with major equations regarding the isotope systematics, the Craig-Gordon model, and mixing. All variables are now defined in the main text and, additionally, a detailed section on terminology and a table summarizing all variables and fractionation factors used within the manuscript are provided in the supplement. Missing information in the sampling section were added and doubling of information given in the Study Area and the Sampling section were removed.

Thirdly, there are three main issues with the results and discussion section, the number of new methods introduced in the results, the amount of significance placed on few data points (vapour compositions), and the limited discussion of the results. Methods introduced in the results section include the HYSPLIT model (results shown without any previous mention of the model), translation ofδ18Op (from OIPC) toδ18Ov, Monte Carlo simulations and fitting of Craig-Gordon to evaporation pan data, and the set-up of sensitivity testing and the evaluation of the sensitivity. These components should all be introduced and described in the methods section. Through the results and discussion section, a lot of weight was placed on the atmospheric vapour compositions which were sampled over two days. While these samples are very important to constrain the Craig-Gordon model and an uncertainty approach has been taken to assess some of the variability, the likelihood of large annual variability and impact should be discussed in more detail rather than discrediting the OPIC on two sample days.

We added a subsection on atmospheric vapour in the methods section, where we now explained why the OIPC model is possibly not suitable for our study site and introduce the HYSPLIT modelling. The sections on the turbulence coefficient and the model sensitivity tests were thoroughly revised so that derived conclusions become clearer and more concise. This discussion should now also clarify why we had placed so much weight on the vapour composition in our previous version. It is a rather critical parameter for the C-G model.

It is certainly not our intention to discredit the OIPC model. The question we raise is if a ‘’precipitation model’’ is applicable to a region where precipitation is virtually absent, which is now better explained. Our small dataset was expanded by one sample and we also back up the data by verifying the measured vapour composition indirectly from the evaporation experiments. As pointed out by the reviewer, constraints on vapour isotopic compositions are very important.

The discussion of the results is limited, particularly with the model uncertainty and the explanation of the dynamics of the salar, in context to the literature. Some ideas that may help the discussion could include (1) the impact of ice and high temperatures on evaporation pans and isotopic fractionation (2) the larger implications of model uncertainty, and(3) discussion on the causes of intra-annual changes of specific ponds (e.g. causes of shifts in d-excess- or 17O-excess-δ18O space in Figs 9 & 10).

We now address these points. In the revised manuscript, we discuss the effect of ice and variable temperatures on the evaporation pans and the effect of sublimation (i.e. reviewers point 1). We have extended the evaluation of model uncertainty (i.e. reviewers point 2). Moreover, we have now included the results of laboratory experiments recently published by Gonfiantini et al. (2020) and compared them with our experimental data, which greatly improves our understanding of the turbulence coefficient. We added a subsection on the isotopic residence times in ponds and lakes at the Salar del Huasco to show that combined triple oxygen and hydrogen isotope systematics do allow inferences on hydrological lake balance and fundamental hydrological processes. Absolute constraints on the timescales of isotopic shifts as a function of pond depth are now provided (i.e. reviewers point 3).

Reply to Referee #2

We again appreciate the helpful comments and suggestions of Reviewer #2. We followed most of these suggestions in the revised version of the manuscript. Please, find below in black the comments of the reviewer, in blue how these are addressed in the revised manuscript.

Having said that, I think that the paper could benefit from a thorough revision of structural aspects to clarify the key messages and conclusions. The paper does mix methods and results in many parts which I think rather confuses the reader. For example, already in the introduction you use a lot of detailed methods including equations 1 and 2 followed by your own results without stating clear research objectives. This might be a bit of a style questions and I see merit in this approach for a theoretical paper, but your paper is based on experimental work in a specific environment and falls out of the former category of scientific works. Therefore, I suggest to more generally introduce the potential utility and challenges of the oxygen-17 tracer in hydrology as this is still not widely used. You could also point towards the fact that you used IRMS and not a laser instrument. I would also urge the authors to present two or three specific objectives for clarity that can be used to guide the reader through the paper.

The structure of the paper has been changed as suggested. We thoroughly revised the introduction and focus now on hydrological processes that determine the isotopic composition of lakes and the larger implication of the 17O-excess parameter as a tool to resolve these processes as well as to identify changes in the hydrological balance of lakes. We used a minimum of equations that are necessary to understand how 17O-excess and d-excess are derived. We now better point out the main objectives of the manuscript to: 1) test the potential of triple oxygen isotope analyses to resolve fundamental hydrologic processes of evaporation and mixing of sources that cannot be resolved by the classical δ^2H-$\delta^{18}O$ analyses; 2) test the robustness of the Craig-Gordon model in a highly dynamic environment with considerable seasonal variability in all the model input parameters; and 3) demonstrate the potential of triple oxygen isotope analyses to derive the hydrological balance of lakes from water isotope and climate monitoring. The fact that we use IRMS and not a laser instrument is stated in the Methods section and in our opinion not relevant enough to be mentioned in the introduction.

In the methods, I found that the HYSPLIT analysis, the OIPC and the E/I modelling is not explained. I would also suggest to present the Craig and Gordon model with equation and in more detail in the methods clearly stating which parameters you varied to assess potential model uncertainty, how exactly you derived the wind turbulence parameter (this appears in the results) and the model experiments you are undertaking to assess the influence of measured atmospheric vapour isotope composition in the model.

In the revised manuscript we have now included a theoretical section with major equations regarding the isotope systematics, the Craig-Gordon model, and mixing. All variables are now defined in the main text and, additionally, a detailed section on terminology and a table summarizing all variables and fractionation factors used within the manuscript are provided in the supplement. Furthermore, we added a subsection on atmospheric vapour and introduce the HYSPLIT modelling. The OPIC model is widely known and explained in detail in the cited literature.

This leads me to suggest separating the results from the discussion and to only use two to three sub-headers that refer back to your specific results rather than at the moment 6 results sub-headers for clarity. These could be grouped according to field experiments, hydrological processes and model experiments as an example.

The revised version of the manuscript now follows a classical structure with separate Results and Discussion, which indeed improves the readability of the text, making key messages clearer. The results section is now divided in three subsections focusing on natural waters in the Salar del Huasco, atmospheric vapour and the isotopic results of pan evaporation experiments. Subsections in the discussion provide now key messages of our data including the determination of the turbulence coefficient from pan evaporation experiment data, the potential of the triple oxygen isotope system to resolve multiple generations of infiltration in groundwater aquifers, and its power to resolve individual hydrological processes of evaporation, recharge and mixing in a most complex and seasonally dynamic lake system.

Triple oxygen isotope systematics of evaporation and mixing processes in a dynamic desert lake system

Claudia Voigt[1], Daniel Herwartz[1], Cristina Dorador[2], Michael Staubwasser[1]

[1]Institute of Geology and Mineralogy, University of Cologne, Zülpicher Str. 49b, 50674 Cologne, Germany
[2]Centro de Biotecnología, Universidad de Antofagasta, Angamos 601, 1270300 Antofagasta, Chile

Correspondence to: Claudia Voigt (c.voigt@uni-koeln.de)

Abstract.

This study investigates the combined hydrogen-deuterium and triple oxygen isotope hydrology of the Salar del Huasco, an endorheic salt flat located on the Altiplano Plateau, N-Chile. The lacustrine system at its center is a hydrologically dynamic and complex system that receives inflow from multiple surface and groundwater sources. It seasonally undergoes flooding, followed by rapid shrinking of the water body in an arid climate with very high evaporation rates. Sampling of ponds, lakes, and recharge sources capture a large range of evaporation degrees. Samples show a range of $\delta^{18}O$ between -13.3 and 14.5 ‰, d-excess between 7 and -100 ‰, and ^{17}O-excess between 19 and -108 per meg. A pan evaporation experiment conducted on-site was used to derive the turbulence coefficient of the Craig-Gordon isotope evaporation model for the local wind regime. This, along with sampling of water vapour at the salar (-21.0 ± 3.3 ‰ for $\delta^{18}O$, 34 ± 6 ‰ for d-excess and 23 ± 9 per meg for ^{17}O-excess) enabled the accurate reproduction of measured ponds and lake isotope data by the Craig-Gordon model. In contrast to classic δ^2H-$\delta^{18}O$ studies, the ^{17}O-excess data not only allow to distinguish two different types of evaporation – evaporation with and without recharge – but also to identify mixing processes between evaporated lake water and fresh flood water. Multiple generations of infiltration events can also be inferred from the triple oxygen isotopic composition of inflow water indicating mixing of sources with different evaporation histories. These processes cannot be resolved using classic δ^2H-$\delta^{18}O$ data alone. Adding triple oxygen isotope measurements to isotope hydrology studies therefore may significantly improve the accuracy of a lake's hydrological balance – i.e. the evaporation-to-inflow ratio (E/I) – estimated by water isotope data and application of the Craig-Gordon isotope evaporation model.

1 Introduction

The majority of water in the hydrologic cycle on Earth represents a dynamic isotopic equilibrium between ocean moisture flux, precipitation, and runoff. However, a number of continental water reservoirs, e.g. lakes in semi-arid or arid environments, may deviate from that state as a result of kinetic evaporation and mixing of sources with different composition (Clark and Fritz, 1997). The Global Meteoric Water Line (GMWL) describes the equilibrium, while the progress of evaporation causes a systematic decrease of ^{17}O-excess and d-excess that is principally predictable by the Craig-Gordon (C-G) isotope evaporation model. The C-G model is the foundation of assessing the hydrological balance, i.e. the evaporation-to-inflow ratio (E/I), of

hat formatiert: Deutsch

hat formatiert: Französisch

hat gelöscht: Triple oxygen isotope measurements are a novel and promising tool in geochemical and hydrological research. This study investigates the combined hydrogen-deuterium and triple oxygen isotope hydrology at the Salar del Huasco, a highly dynamic salt lake system located on the Altiplano Plateau, N-Chile. The region has a semiarid climate that shows strong seasonal and diurnal variability in relative humidity, temperature, and wind conditions. The Salar del Huasco receives inflow from multiple surface sources and groundwater. Episodic flooding after rare rainfall events imposes seasonal fluctuations of the groundwater table and, thus, the lake level. Applying the Craig and Gordon (C-G) evaporation model for triple oxygen isotope data measured along series of increasingly evaporated lakes and ponds within the salar demonstrates the capability to resolve the individual fundamental hydrologic processes of recharge evaporation, simple (pan) evaporation, and transient mixing with surface and subsurface floodwater. Regarding the stream and spring sources, mixing of different generations of recharge is clearly distinguishable from pre-evaporation of a single recharge event. These processes are not resolvable by δ^2H and $\delta^{18}O$ measurements alone. We also show that accurate monitoring of the isotopic composition of ambient water vapour and an estimate of the wind turbulence coefficient in the C-G model are critical aspects required to quantify the hydrologic balance. The wind turbulence coefficient, here 0.54, may be determined accurately from on-site evaporation experiments by fitting evaporation trajectories to the d-excess, $\delta^{18}O$ and residual fraction data.

hat gelöscht: Triple oxygen isotope analysis of ice, lake water, plant water, water structurally bonded in minerals – e.g. gypsum – or minerals exchanging with ambient water during their formation – e.g. amorphous silica and carbonate – have been recognized as a potentially powerful tool in studies of the present and the past hydrologic cycle (e.g. Landais et al., 2006, 2008; Uemura et al., 2010; Surma et al., 2018, 2015; Herwartz et al., 2017; Li et al., 2017; Alexandre et al., 2018, 2019; Evans et al., 2018; Gázquez et al., 2018; Passey and Ji, 2019). The foundations of this tool lie in isotope fractionation theory, which predicts small differences in the relationship between $^{17}\alpha$ and $^{18}\alpha$ during kinetic and equilibrium fractionation (Angert et al., 2004). Later, improvements in analytical procedures (Baker et al., 2002) allowed to resolve these small variations (Barkan and Luz, 2005, 2007). The triple oxygen isotope exponent $\theta = \ln {}^{17}\alpha / \ln {}^{18}\alpha$ was found to be 0.529 for liquid–vapour equilibrium (Barkan and Luz, 2005) and 0.5185 for diffusion of water vapour in air (Barkan and Luz, 2007). Triple oxygen isotope analyses of meteoric water across the globe reveal a curved relationship between $\delta^{17}O$ and $\delta^{18}O$ (Li et al., 2015) defining an average trend line – the Global Meteoric Water Line (GMWL) – similarly to the classic δ^2H–$\delta^{18}O$ system (Luz and Barkan, 2010):¶
$\delta'^{17}O = 0.528 \cdot \delta'^{18}O + 0.000033$ (1)¶
with $\delta'^{x}O = 1000 \cdot \ln(\delta^{x}O/1000 + 1)$. For better visualization of deviations from the GMWL, the ^{17}O-excess parameter has been defined (Luz and Barkan, 2010):¶
$^{17}O - \text{excess} = \delta'^{17}O - 0.528 \cdot \delta'^{18}O$ (2)¶
In natural desert lakes, the progress of evaporation causes a systematic decrease of ^{17}O-excess largely in response to relative humidity. The evaporation trend is principally predictable on regional scale by the classic Craig–Gordon (C-G) isotopic evaporation model (Surma et al., 2015, 2018). The studies by Surma et al. (2015, 2018) also laid out how, besides humidity, other climate variables and hydrological parameters including temperature, wind turbulence, th… [1]

lakes from water isotope measurements. The model variables of the C-G equation – relative humidity, temperature, the isotopic composition of atmospheric vapour, continuous groundwater recharge, wind turbulence above the water surface, and salinity – depend on local climatic conditions and require quantification in order to apply the model (Gonfiantini, 1986; Horita et al., 2008; Gonfiantini et al., 2018). Of these variables, wind turbulence remains beyond determination by direct measurement in the field. Importantly, the mixing of different lake water sources, particularly if these represent precipitation from different seasons or different evaporation histories, presents a significant challenge in deriving the hydrologic balance of lakes from water isotopes in the C-G model that cannot be resolved using classic $^{2}H/^{1}H$ and $^{18}O/^{16}O$ data. Without the means to address wind turbulence and mixing of sources directly, isotope hydrology cannot provide an unambiguous estimate of a lake's hydrological balance.

The analysis of the $^{17}O/^{16}O$ ratio in H_2O in addition to the commonly investigated $^{2}H/^{1}H$ and $^{18}O/^{16}O$ ratios has become an increasingly applied tool in hydrogeological research, because of some favourable properties of the triple oxygen isotope system. For example, while the secondarily derived d-excess parameter [$= \delta^{2}H - 8 \cdot \delta^{18}O$] is largely dependent on relative humidity and temperature, the ^{17}O-excess parameter [$= \delta'^{17}O - 0.528 \cdot \delta'^{18}O$ with $\delta' = 1000 \cdot (\delta/1000+1)$] has shown to be temperature insensitive in the natural range between 11-41°C (Barkan and Luz, 2005; Cao and Liu, 2011). Also, the effect of high salinity on the evaporation trajectory of the C-G model is less significant (Surma et al., 2018). Hence, the combined analysis of $\delta^{17}O$, $\delta^{18}O$ and $\delta^{2}H$ provides information on fundamental processes of the hydrological cycle such as humidity, moisture sources, evaporation conditions and mixing, which would be masked by temperature variability if $\delta^{18}O$ and $\delta^{2}H$ were analysed alone (Angert et al., 2004; Barkan and Luz, 2005, 2007; Landais et al., 2006, 2008, 2010; Surma et al., 2015, 2018; Herwartz et al., 2017). As such, the general potential of the ^{17}O-excess parameter as a tool to quantitatively reconstruct paleo-humidity from plant silica particles (Alexandre et al., 2018, 2019) and lake sediments (Evans et al., 2018; Gázquez et al., 2018) could be demonstrated.

The seasonal dynamics in climate variables, flooding, and their respective effect of mixing on the triple oxygen isotope composition of lakes have not yet been investigated. To examine these factors and ultimately to test the robustness of the C-G model as a reliable monitoring tool for the lake hydrologic balance in a most complex and highly dynamic desert lake system, we measured the isotopic data from springs, ponds and lake water samples from the Salar del Huasco, N-Chile, covering a 300 ‰ salinity range, and compared them with evaporation trajectories modelled for local seasonal conditions. All variables of the C-G model were constrained by meteorological data from an on-site weather station, a pan evaporation experiment, isotopic measurements of atmospheric water vapour samples and inflowing water sources. Due to the extreme dynamics in climatic and hydrological parameters, the Salar del Huasco provides an ideal environment to test the potential of triple oxygen isotope analyses in resolving different hydrological processes like permanent recharge and highly episodic mixing with flood water and to identify changes in the hydrological balance of lakes.

2 Study Area

The Salar del Huasco is an endorheic salt flat located in the south of a longitudinal volcano-tectonic depression at the western margin of the Chilean Altiplano at about 3770 m (Fig. 1). It covers an area of about 50 km² but only 5 % of the surface is permanently covered by water (Risacher et al., 2003). The hydrological balance of the salar is controlled by a shallow groundwater table, perennial streams, rare and highly seasonal precipitation, and episodic injection of runoff water after heavy rainfalls or snowmelt. The environment is characterized by exceptionally high evaporation rates and high variability in relative humidity and temperature throughout the year with considerable diurnal amplitude.

An on-site weather station (20°15.42'S 68°52.38'W) is operated by the Centro de Estudios Avanzados en Zonas Áridas (CEAZA) at the north-western margin of the salar since September 2015 (CEAZA, 2020). Over this period, mean annual relative humidity and temperature are 41 % and 5°C, respectively. Both relative humidity and temperature are highly variable throughout the year with mean seasonal values of 54 % and 8°C in austral summer (Dec–Mar) and 33 % and 2°C in austral winter (Jun–Sep). Day-night fluctuations range between 0 and 99 %, and from -19°C to 23°C. Mean annual wind speed is about 2.5 $m \cdot s^{-1}$, most times coming from S to SW direction. Typically, it is calm in the morning, but very windy in the afternoon with 5 $m \cdot s^{-1}$ average wind speed and gusts up to 24 $m \cdot s^{-1}$.

Long-term mean annual precipitation is 150 $mm \cdot a^{-1}$, but interannual variability is high due to their dependence on wind patterns (Garreaud and Aceituno, 2001; Risacher et al., 2003). Precipitation occurs mainly in austral summer (Dec–Mar) and is related to easterly airflow from the Atlantic Ocean and the Amazon Basin (e.g. Aravena et al., 1999; Garreaud et al., 2003; Houston, 2006). In contrast, less frequent winter rains and snow are associated with the interaction of cold air masses from the Pacific with tropical air masses from the Amazon Basin (Aravena et al., 1999). The intensity of convective storms and variability of the continental effect in the Amazon Basin lead to significant isotopic variability in summer rains (Aravena et al., 1999). In contrast, winter rains comprise generally higher $\delta^{18}O$ values and are isotopically less variable (Aravena et al., 1999). This may be attributed to lower variability in the contribution of pre-evaporated water from the Amazon Basin in the dry season and the non-convective nature of winter storms.

The hydrogeological system of the Salar del Huasco consists of three aquifers, where the upper and the intermediate aquifer are located in the basin's sediment infill, separated by a thin aquitard, and the lower aquifer is formed in volcanic bedrock (Acosta and Custodio, 2008). The upper aquifer is recharged by the Collacagua river that drains the northern part of the basin and completely infiltrates 10 km before reaching the salar (Acosta and Custodio, 2008). In periods of heavy rainfall, the river directly flows into the salar leading to widespread flooding of the northern area (Fig. 2e). Several springs and creeks around the salar and the shallow groundwater table contribute to the formation of perennial lakes. Furthermore, ephemeral ponds emerge episodically due to precipitation, surface and subsurface runoff and a rising groundwater table in the rainy season. Variable groundwater and stream sources, episodic precipitation and surface runoff, and ephemeral flooding in austral summer result in a highly dynamic system with strongly fluctuating lake level.

hat nach unten verschoben [1]: The environment is characterized by exceptionally high evaporation rates and high variability in relative humidity and temperature throughout the year with considerable diurnal amplitude.

hat gelöscht: An on-site weather station provides records of local weather data. In addition, we were able to constrain relevant variables from the C–G model equation by in-situ pan evaporation experiments. Springs around the Salar del Huasco were sampled to evaluate isotopic variability of inflowing water sources. We show evaporation trajectories modelled for seasonal conditions at the Salar del Huasco in comparison to measured isotope data from water samples covering a 300 ‰ salinity range. This study identifies many aspects of the seasonal dynamics in this complex hydrological system that influence the isotopic composition of natural ponds at the Salar del Huasco. We also demonstrate that triple oxygen isotope analyses, in contrast to classic δ^2H and $\delta^{18}O$ measurements, can distinguish different major hydrological processes like recharge and mixing and allow to identify changes in the hydrological balance of lakes.¶

hat verschoben (Einfügung) [1]

hat verschoben (Einfügung) [2]

hat gelöscht: Mean annual values of relative humidity and temperatures are 42 % and 4°C, respectively (CEAZA, 2019). Both relative humidity and temperature are highly variable throughout the year with mean seasonal values of 59 % and 8°C in austral summer (Dec–Mar) and 34 % and 1°C in austral winter (Jun–Sep) (CEAZA, 2019). Day-night fluctuations range between 1 and 99 %, and from -19°C to 22°C (CEAZA, 2019). Mean annual wind speed is about 2.5 $m \cdot s^{-1}$, most times coming from S to SW direction (CEAZA, 2019). Typically, it is calm in the morning, but very windy in the afternoon with 4 $m \cdot s^{-1}$ average wind speed and gusts up to 20 $m \cdot s^{-1}$ (CEAZA, 2019).¶
Precipitation occurs mainly in austral summer (Dec–Mar), where it is often of convective nature and

hat verschoben (Einfügung) [3]

hat verschoben (Einfügung) [4]

hat nach oben verschoben [2]: Long-term mean annual precipitation is 150 $mm \cdot a^{-1}$, but interannual variability is high due to their dependence on wind patterns (Garreaud and Aceituno, 2001; Risacher et al., 2003).

hat gelöscht: can

hat gelöscht: flow

hat gelöscht: ¶

hat gelöscht: Based on satellite images and field observations, six main hydrological subsystems could be identified (Fig. 2). Three springs at the western part of the salt flat and one at the south-eastern margin establish two perennial lake systems – *Laguna Grande* and *Laguna Jasure* (Fig. 2b). A channel originating from the *Laguna Grande* extends along the southern margin of the salt flat. This connection may contribute to flooding of southern areas during lake ... [2]

hat nach unten verschoben [5]: area may become widely flooded in austral summer (Fig. 2e) but dries up rapidly after the rainy season (Fig. 2g).

hat gelöscht: The northern subsystem is at least temporarily connected to the south-eastern system as indicated by a small channel observed in satellite images. A minor subsystem in the north-western ... [3]

3 Sampling

Natural water samples from the Salar del Huasco were taken during field campaigns in September 2017, September 2018, and March 2019 (Fig. 2 and Table S2). The sample set includes springs, perennial lakes (*Laguna Grande* in the W, and *Laguna Jasure* in the SE) and ephemeral ponds of which several were apparently recharged and some apparently stagnant. Lakes and ponds are all very shallow (5–30 cm). Samples were taken from the water surface, and temperature, pH and conductivity were measured on site using a digital precision meter *Multi 3620 IDS*.

Based on satellite images and field observations, five major hydrological subsystems could be identified (Fig. 2). The *Laguna Grande* in the western part of the salt flat is intermediate saline with values varying seasonally between about 20 and 35 $g \cdot l^{-1}$. A channel originating from the southern end of this lagoon extends along the southern margin of the salt flat. This channel contributes to flooding of the southern area during the rainy season, while lowering of the water table over the course of the year leads to isolation of ponds (Fig. 2e and g). The large range in salinity (1 – >100 $g \cdot l^{-1}$) observed in shallow lakes and ponds at the south to south-western margin of the salar may indicate that their hydrological balance alternates between recharge and isolation.

In the south-eastern area, a perennial spring fed a chain of lakes with generally low salinity < 2 $g \cdot l^{-1}$. Some ponds were visibly connected by streams and creeks. Others located closer to the eastern margin of the salt flat, were topographically elevated and therefore isolated from the main south-eastern inflow. Satellite images indicate that ponds closer to the salar's centre may represent a mixture of source water from the south-eastern inflow and a further subsystem in the north (Fig. 2e).

The northern subsystem is probably fed by subsurface inflow of the Collacagua river. Its area may become widely flooded in austral summer (Fig. 2e) but dries up rapidly after the rainy season (Fig. 2g). Ponds from the northern area sampled in 09/17 were characterized by an extreme salinity gradient from 2 to 343 $g \cdot l^{-1}$, broadly decreasing from east to west (Table S2). These ponds were often salt-encrusted and showed black, sulphur-reducing microbial mats at the bottom. In 03/19, this entire area was covered by a large low-salinity lake.

In the north-western area, a spring originating from a small, vegetated hill fed a series of ponds with salinities < 1 $g \cdot l^{-1}$. An adjacent chain of ponds sampled in 09/17 about 750 m to the south-east with salinities between 1 and 6 $g \cdot l^{-1}$ was not visibly connected to this spring and must have been sustained by the shallow groundwater table. Three topographically elevated ponds close to the margin had higher salinity of 8 to 40 $g \cdot l^{-1}$. The area around these ponds was more vegetated, indicating that they were older, i.e. represented an earlier flooding but became isolated from recharge. Despite extensive rainfall-induced-flooding in February 2019, the north-western part of the salt flat was almost dry in March 2019.

Besides water samples from surface waters, we sampled atmospheric vapour using a Stirling cooler cycle system (*Le-Tehnika*, Kranj, Slovenia) built after Peters and Yakir (2010). Sampling was carried out on three days during field campaigns in 09/17 and 03/19 (Table 1). Atmospheric vapour was sampled at ground level. Water vapour was captured by streaming air with a flow rate of 600-800 $ml \cdot min^{-1}$ through a 4 ml vial, which was attached to the cold finger of the Stirling cooler and insulated.

hat nach unten verschoben [6]:). Water temperatures measured during sampling were found to be up to 5°C lower than ambient air temperatures. However, during midday, temperatures of water may exceed air temperatures by several degrees due to solar heating of the pans.

hat gelöscht: Pan evaporation experiments with 600 ml, 800 ml, and 1000 ml of fresh water (0.805 $mS \cdot cm^{-1}$) filled in stainless steel evaporation pans (Ø 20 cm) were carried out on site over a period of three days. Samples were taken every day around 18:00 and, additionally, at the third day after 13:00. The pan filled with 600 ml fresh water, dried up before the end of the experiment so that no sample could be taken in the evening of the last day. Air temperature, relative humidity, and wind speed were monitored locally at the experiment using a *Kestrel 5500 weather meter* (Fig. S1). Mean relative humidity and temperature are 4°C and 35 % over the whole period of the experiment. As temperatures dropped below 0°C in the night, a considerable fraction, if not all, of the water in the pans froze during the night leading to either a solid ice block or a thick ice layer above the remaining liquid. Consequently, evaporation from pans was mostly restricted to daytime. The effective evaporation time interval was assumed to last from 9:30 to 23:30 – the period when T > 0°C. During that time, average air temperature and relative humidity were 11°C and 21 % with extreme values of 23°C and 7 % occurring just after midday (Fig. S1

hat gelöscht: The wind was very strong between 12:00 and 19:00 with an average wind speed of 5 $m \cdot s^{-1}$ and gusts up to 14 $m \cdot s^{-1}$ coming from S to W direction, i.e. the general direction of the Pacific coast.¶

hat gelöscht: S1

hat gelöscht: ,

hat gelöscht:

hat gelöscht: the northern Collacagua

hat verschoben (Einfügung) [5]

hat gelöscht: S1

hat gelöscht: these ponds

hat formatiert: Schriftfarbe: Akzent 3

hat gelöscht: Additional samples were taken from shallow lakes and ponds at the south to south-western margin of the salar. Satellite images and field observations indicate that this area is flooded by branches of the Laguna Grande during the rainy season and that lowering of the water table over the course of the year leads to isolation of ponds (Fig. 2e and g).¶

hat gelöscht: Sampling was carried out on the 20.09.17 and the 21.09.17 during the evening from about 18:00 to 21:00 using an air-flow rate of 600–800 $ml \cdot min^{-1}$

Extremely low absolute humidity values at the Salar del Huasco required sampling over several hours to yield 0.1-0.2 µl of atmospheric vapour.

Additionally, pan evaporation experiments with 600 ml, 800 ml, and 1000 ml of fresh water (0.805 mS·cm^{-1}) filled in stainless steel evaporation pans (Ø 20 cm) were carried out on-site over a period of three days (20°15.4'S 68°52.4'E). The rationale behind this experimental design was to account for the extreme diurnal and significant average day-to-day variability of all variables in the C-G model by letting evaporation progress over several days. By varying the initial volume, we were able to achieve a wide spread of fractional evaporative water loss. Samples were taken every day around 18:00 and, additionally after 13:00 on the third day. The pan filled with 600 ml fresh water, dried up before the end of the experiment so that no sample could be taken in the evening of the third day. Air temperature, relative humidity, and wind speed were monitored locally at the experiment at about 1.5 m above ground using a *Kestrel 5500 weather meter* (Fig. S2). Mean relative humidity and temperature were 4°C and 35 % over the whole period of the experiment. As temperatures dropped below 0°C in the night, a considerable fraction, if not all, of the water in the pans froze during the night. This led to the formation of either a solid ice block or a thick ice layer above the remaining liquid. Consequently, evaporation from pans was mostly restricted to daytime when samples were thawed. The effective evaporation time interval was assumed to correspond to the period when T > 0°C, resulting in average air temperature and relative humidity values of 10°C and 22 % (Fig. S2). Water temperatures measured during sampling were found to be up to 5°C lower than ambient air temperatures. However, during midday, temperatures of water may exceed air temperatures by several degrees due to solar heating of the pans. Winds were very strong between 12:00 and 19:00 with an average wind speed of 5 m·s^{-1} and gusts up to 14 m·s^{-1} coming from S to W direction.

hat verschoben (Einfügung) [6]

4 Methods

4.1 Isotope and chemical analyses

The hydrogen and triple oxygen isotope composition of water samples were analysed by isotope ratio mass spectrometry (IRMS). Complementary concentration data of Na^+, K^+, Ca^{2+}, Mg^{2+}, Cl^-, and SO_4^{2-} in natural samples were determined by ICP-OES (Table S2). A short discussion of the chemical data is provided in the supplement (T2, Fig S7).

hat gelöscht: see Fig. S6 and Table S1

Hydrogen isotope ratios are measured by continuous-flow IRMS of H_2. Water samples are injected in a silicon carbide reactor (*Heka-Tech*, Wegberg, Germany) that is filled with glassy carbon and heated to 1550°C, where they are reduced to H_2 and CO. The produced gases are carried in a helium gas stream (100 130 ml·min^{-1}), separated by gas chromatography (GC) and finally introduced in a *Thermo Scientific MAT 253* mass spectrometer for hydrogen isotope analysis. The long-term external reproducibility (SD) is about 0.9 ‰ and 1.15 ‰ for δ^2H and d-excess, respectively.

hat gelöscht: separated

hat gelöscht: –

hat gelöscht:)

hat gelöscht: , are

For triple oxygen isotope analysis, water samples are fluorinated, followed by dual-inlet IRMS of O_2. The method is described in detail in Surma et al. (2015) and Herwartz et al. (2017). In brief, 2.8 µl of water are injected in a heated CoF_3 reactor (370°C) that is continuously flushed with helium (30 ml·min^{-1}). The produced oxygen gas is cryogenically purified and trapped in one of twelve sample tubes of a manifold. The manifold is connected to a *Thermo Scientific MAT 253* for dual-inlet IRMS analysis.

The long-term external reproducibility (SD) is about 0.12 ‰, 0.25 ‰ and 8 per meg for $\delta^{17}O$, $\delta^{18}O$ and ^{17}O-excess, respectively. All isotope data herein are reported on SMOW–SLAP scale (Schoenemann et al., 2013). The scale is usually contracted using the setup described herein. This can partly be attributed to blank contribution (Herwartz et al., 2017). We observe an increase in scale contraction over the usage period of a CoF_3 reactor filling and a reduction of precision and accuracy of isotopic data, indicating that the blank contribution increases with time. To account for this effect, SMOW–SLAP scaling was performed daily using internal standards. Isotope measurements with anomalous high scaling factors or standard deviations were discarded.

4.2 The Craig-Gordon isotope evaporation model at the Salar del Huasco

The Craig-Gordon (C-G) isotope evaporation model forms the basis for numerous models describing the isotopic composition of natural lakes (e.g. Gonfiantini, 1986; Gat and Bowser, 1991; Horita et al., 2008). There are two principal evaporation scenarios – one without recharge (hereinafter termed 'simple evaporation') and one with continuous recharge (hereinafter termed 'recharge evaporation') (Craig and Gordon, 1965; Criss, 1999; Horita et al., 2008). In the case of simple evaporation, the isotopic composition of the lake is only controlled by the degree of evaporation (Fig. 3; Gonfiantini et al., 2018):

$$R_W = f^B \cdot \left(R_{WI} - \frac{A}{B} \cdot R_V\right) + \frac{A}{B} \cdot R_V$$

where R_{WI} denotes the initial isotopic composition of the water body, R_V is the isotopic composition of atmospheric vapour, and f is the fraction of residual water. The parameters A and B describe the isotopic fractionation associated with evaporation in dependence on the relative humidity h normalized to the water surface temperature:

$$A = -\frac{h}{\alpha^n_{diff,\,l-v} \cdot (1-h)}$$

$$B = \frac{1}{\alpha_{eq,\,l-v} \cdot \alpha^n_{diff,\,l-v} \cdot (1-h)} - 1$$

In the case of recharge evaporation, the isotopic effect of continuous inflow is accounted for by the evaporation-to-inflow-ratio (E/I) (Fig. 3; Criss, 1999):

$$R_{WS} = \frac{\alpha_{eq,\,l-v} \cdot \alpha^n_{diff\ \ l-v} \cdot (1-h) \cdot R_{WI} + \alpha_{eq,\,l-v} \cdot h \cdot E/I \cdot R_V}{E/I + \alpha_{eq,\,l-v} \cdot \alpha^n_{diff,\,l-v} \cdot (1-h) \cdot (1-E/I)}$$

Here, R_{WI} refers to the isotopic composition of the inflowing water. Under steady-state conditions $E/I \leq 1$, whereas the lake begins to desiccate when evaporation exceeds the inflow ($E/I > 1$).

Diffusive ($\alpha_{diff,\,l-v}$) and equilibrium ($\alpha_{eq,\,l-v}$) isotope fractionation cause a systematic increase in $\delta^{18}O$ and decrease in d-excess and ^{17}O-excess with progressive evaporation. A detailed description of all variables used herein is given in the supplement (T1, Table S1). The effect of wind turbulence – which leads to variable proportions of diffusive and turbulent isotope fractionation in dependence of wind speed – is accounted for by inserting a correcting exponent to the diffusive fractionation factor, $\alpha_{diff,\,l-v}^n$ (Dongmann et al., 1974). The turbulence coefficient n can vary between 0 (fully turbulent atmosphere) and 1

hat gelöscht: which may indicate

hat gelöscht: 5

hat gelöscht: –

hat gelöscht: isotopic

Formatiert: Überschrift 2

hat gelöscht: The classic evaporation theory distinguishes two principal evaporation scenarios, one with recharge (recharge evaporation) and one without recharge (simple evaporation) (Craig and Gordon, 1965; Criss, 1999; Horita et al., 2008). The C–G model does not account for mixing processes, e.g. as a result of flooding or snowmelt, but can be used to calculate such effect by applying mass balance. The three trajectories are principally resolvable in triple oxygen isotope space, whereas in δ^2H–$\delta^{18}O$ space they tend to merge within data uncertainty (Fig.

hat nach unten verschoben [7]: 3). All three trajectories can be expected in a dynamic arid hydrological setting such as the Salar del Huasco. Water affected exclusively by evaporation must progress along either of the two principal evaporation trajectories defined by the C

hat gelöscht: –G model. Episodic flooding after rainfall events are detectable on satellite images of Salar del Huasco (Fig. 2). Thus, mixing processes are likely, but should only be transient due to the rarity of flooding events.¶
The major variables determining the isotopic composition of evaporating water (i.e. residual water) are relative humidity (*h*), temperature (*T*) and wind-induced turbulence (an empirically determined coefficient *n*) along with the isotopic composition of ambient atmospheric vapour (δ_V), and initial or inflowing water (δ_{WI}

hat gelöscht: The effect of wind turbulence – which is related to

hat gelöscht: –

hat formatiert: Schriftart: Nicht Kursiv

hat gelöscht: theoretically

(calm atmosphere), but typically assumes values of $n \geq 0.5$ under natural conditions (Gonfiantini, 1986; Mathieu and Bariac, 1996; Surma et al., 2018). Recent laboratory experiments suggest that part of the evaporating water is removed by spray and microdroplet vaporization without any isotope fractionation when wind speed exceeds ~0.5 $m \cdot s^{-1}$, which may require a modification of the above described C-G approach (Gonfiantini et al., 2020). We evaluated the effect of a possible partial evaporative water loss without fractionation on the simple evaporation trajectory by introducing a 'virtual outlet' f_{out} in the isotopic mass balance equation, which finally results in a modification of the parameter B:

$$B_{out} = \frac{1 - f_{out}}{\alpha_{eq,\,l-v} \cdot \alpha^{n}_{diff,\,l-v} \cdot (1 - h)} + \frac{f_{out}}{(1 - h)} - 1$$

Salinity affects isotope activities and increases fluid viscosity thereby decreasing the vapour pressure above the water body. In the C-G model, this may be accounted for by correcting equilibrium fractionation factors for the classic salt effect (Horita, 1989, 2005; Horita et al., 1993) and using effective rather than actual relative humidity. This effect requires consideration within the δ^2H-$\delta^{18}O$ system at salinities > 100 $g \cdot l^{-1}$ and is much less significant for the $\delta^{17}O$-$\delta^{18}O$ system (Sofer and Gat, 1972, 1975; Horita, 1989, 2005; Surma et al., 2018). To avoid unnecessary complication of the more principal approach of this study, salinity effects were neglected in our model calculations.

The C-G model does not account for mixing processes, e.g. as a result of flooding or snowmelt, but can be used to calculate such effect by applying mass balance: $\delta X_{mix} = f \cdot \delta X_1 + (1\text{-}f) \cdot \delta X_2$, where δX_1 and δX_2 represent the isotopic composition of two different water sources and δX_{mix} is the isotopic composition of the resulting mixed water body with X denoting ^{18}O, ^{17}O, or ^{2}H, respectively. Mixing curves are inversely shaped to the evaporation trajectories in triple oxygen isotope space (Fig. 3). At the Salar del Huasco mixing may occur episodically due to flooding and fluctuations in the groundwater level as detectable on satellite images (Fig. 2). Such mixing processes should be transient due to the rarity of flooding events. In our model approach, we assume that the isotopic composition of the admixed water is similar to that of spring water, which approximates the isotopic composition of groundwater reasonably well (Uribe et al., 2015).

Simple evaporation, recharge evaporation and mixing are principally well resolvable in triple oxygen isotope space, whereas in δ^2H-$\delta^{18}O$ space, they tend to merge within data uncertainty (Fig. 3). All three trajectories can be expected in a dynamic arid hydrological setting such as the Salar del Huasco. Water affected exclusively by evaporation must progress along either of the two principal evaporation trajectories defined by the C-G model, depending on the recharge conditions. On the other hand, episodic flooding events initiate mixing leading to transient deviations from these general evaporation trends. The relative isotopic difference between inflowing water (δ_{WI}) and atmospheric vapour (δ_V) mainly determines the resolution of evaporation trajectories for different relative humidity in the triple oxygen isotope plot (Surma et al., 2018). For the given boundary conditions at the Salar del Huasco, evaporation trajectories show low sensitivity to changes in relative humidity, temperature, and the turbulence coefficient in the diagram of ^{17}O-excess over $\delta^{18}O$ (Fig. S3). Thus, seasonal and diurnal variability in these climate variables should have a low impact on the triple oxygen isotope composition of lakes and ponds at the Salar del Huasco, which is favourable for the purpose of this study to resolve different hydrological processes of evaporation, recharge, and mixing.

hat formatiert: Schriftart: Nicht Kursiv

hat gelöscht: -

hat gelöscht: However, this effect only requires consideration in the δ^2H–$\delta^{18}O$ system at salinities > 100 $g \cdot l^{-1}$ and was therefore neglected in our model calculations (Sofer and Gat, 1972, 1975; Horita, 1989, 2005).

hat verschoben (Einfügung) [8]

hat verschoben (Einfügung) [7]

hat gelöscht: -

hat gelöscht: 4

hat gelöscht: supporting

4.3 The isotopic composition of atmospheric vapour

A few atmospheric vapour samples were extracted on-site using a battery-powered Stirling cooler (Peters and Yakir, 2010). Due to the low relative humidity at the study site, extractions lasted 2-3 hours and only three samples could be taken.

In the absence of sufficiently abundant direct measurements, the isotopic composition of atmospheric vapour may be inferred from precipitation data, e.g. derived from the Online Isotope in Precipitation Calculator (OIPC) (Bowen, 2020), assuming isotopic equilibrium [$\delta X_V = (\delta X_P+1000)/\alpha_{eq,\ l\text{-}v}-1000$, where δX_P refers to the isotopic composition of precipitation and X denotes ^{18}O, ^{17}O, or ^{2}H, respectively]. However, the applicability of the equilibrium assumption is questionable for the Salar del Huasco, where precipitation mostly occurs in rare thunderstorm events originating from easterly sources. More importantly, rain samples cannot be representative for the local vapour because throughout the majority of the year air masses originate from westerly Pacific sources, which generally do not lead to precipitation (Garreaud et al. 2003). To confirm the predominant western origin of vapour for the time of this study, the HYSPLIT Lagrangian model (Stein et al., 2015) was used to calculate seven-day air mass back-trajectories in daily resolution (12:00) for the month prior to each of the sampling campaigns for ground level (3800 m above sea level (asl)) and 1500 m above ground (5300 m asl) (c.f. Aravena et al., 1999). Additionally, air mass back-trajectories were modelled in hourly resolution for the time of vapour sampling to confirm the Pacific origin of sampled vapour. Because direct vapour extraction in the arid environment requires several hours of attendance, we were only able to extract a limited number of point-in-time samples. To augment the scarce data base, we verified our $\delta^{18}O_V$ indirectly from the on-site evaporation experiments.

5 Results

5.1 Natural waters in the Salar del Huasco basin

Springs sampled in 09/17 comprise average values of -12.45 ± 0.64 ‰ for $\delta^{18}O$, 2.2 ± 2.9 ‰ for d-excess, and 11 ± 7 per meg for ^{17}O-excess, which are in good agreement with published isotopic data of springs and wells in the Salar del Huasco basin (-12.56 ± 1.36 ‰ in $\delta^{18}O$ and 3.2 ± 5.7 ‰ in d-excess; data from Fritz et al., 1981; Uribe et al., 2015; Jayne et al., 2016). The springs' isotopic composition shows slight intra- and interannual variability comprising average $\delta^{18}O$, d-excess and ^{17}O-excess values of -12.31 ± 0.50 ‰, 1.3 ± 2.2 ‰ and 6 ± 7 per meg in 09/18 and -12.55 ± 0.68 ‰, 5.5 ± 2.0 ‰, and 2 ± 6 per meg in 03/19, respectively. The Collacagua river, which was sampled at about 15 km distance from the salar, revealed similar isotopic composition with $\delta^{18}O$, d-excess and ^{17}O-excess values of -12.38 ‰, 1.6 ‰ and 5 per meg in 09/18 and -12.45 ‰, 5.8 ‰ and 5 per meg in 03/19, respectively.

The ponds in the Salar del Huasco generally comprise increasing $\delta^{18}O$ values with decreasing d-excess and ^{17}O-excess values ranging from -11.23 to 14.50 ‰ in $\delta^{18}O$, from -1.3 to -100.4 ‰ in d-excess, and from 19 to -108 per meg in ^{17}O-excess (Fig. 4). Ponds from the north-western and south-eastern subsystem are generally less enriched in $\delta^{18}O$ compared to ponds from the northern subsystem. Ponds in the south-western area span a wide range in isotopic composition from -5.54 ‰ to about 14.5 ‰,

hat gelöscht: In this study, four of the five variables in the C–G equation are known from monitoring (T, h) and direct measurements (δ_W, δ_V). The turbulence coefficient n is not easily obtainable from wind speed monitoring but can be accurately derived from the evaporation experiment (see Section 6.2). The vapour composition (δ_V) was measured directly but could be more variable over the sampling period than our two days of measurement suggest. There may only be a weak relationship on average between vapour and rainfall composition at the Salar del Huasco. High-precipitation events in austral summer show significant isotopic variability that is related to a variable continental effect in the Amazon Basin and the intensity of convective storms

including the highest $\delta^{18}O$ values observed in our sample set. The permanent Laguna Grande has a composition in the intermediate range of all investigated ponds showing considerable seasonal and intra-annual variability between -4.15 and 3.2 ‰ in $\delta^{18}O$, -1.9 and -41.9 ‰ in d-excess, and -15 and -39 per meg in ^{17}O-excess.

5.2 Atmospheric vapour

Two atmospheric vapour samples taken during the field campaign in 09/17 yield in average -19.4 ± 2.3 ‰ for $\delta^{18}O_V$, 30 ± 3 ‰ for d-excess$_V$ and 18 ± 2 per meg for ^{17}O-excess$_V$. An additional vapour sample taken in 03/19 comprise a slightly more depleted $\delta^{18}O_V$ value of -24.3 ‰, and d-excess$_V$ and ^{17}O-excess$_V$ values of 41 ‰ and 33 per meg, respectively. The overall average of all three measurements is -21.0 ± 3.3 ‰, 34 ± 6 ‰ and 23 ± 9 per meg for $\delta^{18}O_V$, d-excess$_V$ and ^{17}O-excess$_V$, respectively.

Seven-day air mass back-trajectories calculated using the HYSPLIT model suggest that air masses during vapour sampling were mainly derived from Pacific sources (Fig. 5). A predominantly western origin of air masses for the month prior to sampling is confirmed by 7-day air mass back-trajectories (Fig. 5). These model results support the assumption that direct vapour measurements reflect the mean annual isotopic composition of atmospheric vapour at the Salar del Huasco.

The measured mean $\delta^{18}O_V$ value of -21.0 ± 3.3 ‰ is comparable to the mean annual $\delta^{18}O_V$ value of -21.8 ‰ calculated based on monthly precipitation data derived from the OIPC database (Bowen et al., 2005). The apparent similarity between the OIPC model and our measurements may be coincident resulting from the seasonality of precipitation sources with a major contribution of the depleted Amazon moisture source and a minor contribution of the relatively enriched winter snow moisture source (cf. Aravena et al., 1999).

5.3 Pan evaporation experiments and the determination of the local turbulence coefficient

Water samples from the evaporation experiments comprise increasing $\delta^{18}O$ and decreasing ^{17}O-excess and d-excess values with increasing degree of evaporation (Fig. 6). The observed trends are consistent between experiments carried out with different initial volume. The isotopic composition of the initial water was -10.96 ‰, 4.4 ‰ and 16 per meg, for $\delta^{18}O$, d-excess and ^{17}O-excess, respectively. Over the three-days experimental period, the largest enrichment in $\delta^{18}O$ (Δ = 31.44 ‰) and depletion in d-excess (Δ = -119.6 ‰) and ^{17}O-excess (Δ = -155 per meg) is observed for the evaporation pan with the lowest initial volume (600 ml), which reflects the maximum fractional loss by evaporation relative to the initial volume.

The pan evaporation experiment data was used to empirically determine the turbulence coefficient n – a parametrized value that is not directly obtainable from wind speed data. In a plot of d-excess over the fraction of remaining water, the evaporation trajectory is predominantly affected by the magnitude of the turbulence coefficient (Fig. 7a), and only barely sensitive to the other variables of the C-G equation (Fig. S3). Hence, the turbulence coefficient can be accurately estimated by finding the value with that the modelled trajectory fits through all experimental data. Importantly, this approach is insensitive to $\delta^{18}O_V$, the variable that is most difficult to measure (Fig. 7b).

hat nach oben verschoben [3]: (Aravena et al., 1999).
hat gelöscht: Winter rains comprise generally higher $\delta^{18}O$ values and are isotopically less variable than summer rains. This may be attributed to less variability in the contribution of pre-evaporated water from the Amazon Basin in the dry season and the non-convective nature of winter storms
hat nach oben verschoben [4]: (Aravena et al., 1999).
hat gelöscht: The isotopic composition of winter rains reflects a mixture of moisture from air masses originating from the Amazon Basin and from the Pacific Ocean, while the mean annual isotopic composition of atmospheric vapour over the Salar del Huasco basin is dominated by air masses derived from Pacific sources (Garreaud et al., 2003).¶
6 Results and discussion¶
6.1
hat gelöscht: Atmospheric
hat gelöscht: was sampled on 20.09.17 and 21.09.17. Measurements revealed an
hat gelöscht: $\delta^{18}O_V$ of
hat gelöscht: ‰. Average
hat gelöscht: -
hat gelöscht: -
hat gelöscht: are 30 ± 3
hat gelöscht: 18 ± 2
hat gelöscht:
hat gelöscht: S3
hat gelöscht: vapour is
hat gelöscht: for the time of our sampling campaign in 09/17
hat gelöscht: for the month prior to sampling using the HYSPLIT ... [4]
hat gelöscht: model's mean annual $\delta^{18}O_V$ value of -21.8 ‰
hat gelöscht: However,
hat gelöscht: estimate is based on two fundamentally different
hat gelöscht: processes, where on one hand there is
hat gelöscht: with convective summer rain, high rainout and ... [5]
hat gelöscht: on the other hand
hat gelöscht: These two seasonal aspects coincidently combine ... [6]
hat gelöscht: 6.2
Formatiert: Überschrift 2
hat gelöscht: ¶ ... [7]
hat gelöscht: isotope diagrams were modelled for pan ... [8]
hat nach unten verschoben [9]: 6b).
hat gelöscht: A Monte Carlo error simulation yields n = 0.44 ... [9]
hat nach unten verschoben [10]: The fraction of total
hat gelöscht: In our experimental setup, this essentially equals ... [10]

Using model input parameters summarized in Table 2, fitting the evaporation model through all experimental data in the plot of d-excess over the fraction of remaining water implies n = 0.44 ± 0.04. This value falls within error in the lowermost range of turbulence coefficients ≥ 0.5 that are typically observed under natural conditions world-wide (Merlivat and Jouzel, 1979; Gonfiantini, 1986; Mathieu and Bariac, 1996; Surma et al., 2018; Gázquez et al., 2018) and apparently reflects excessive evaporation during midday at prevailing strong winds with gusts up to 24 $m \cdot s^{-1}$. However, laboratory experiments carried out by Gonfiantini et al. (2020) revealed that fitting the evaporation trajectory independently to $\delta^{18}O$ and $\delta^{2}H$ data results in a discrepancy between the individually derived turbulence coefficients at wind speeds above 0.5 $m \cdot s^{-1}$. Accordingly, $\delta^{18}O$ and $\delta^{2}H$ data of our evaporation experiment may only fit the C-G model at an unrealistically low value of of n = 0.34 for $\delta^{18}O$, while no fit can be achieved for any value of $0 \leq n \leq 1$ in the diagram of $\delta^{2}H$ vs the residual fraction (Fig. 8).

In this particular experiment, the freezing at night-time might have biased the relationship between d-excess and the fraction of remaining water. When the ice begins to melt in the morning, a considerable fraction, if not the whole resulting water film on top of the pan's frozen surface layer may evaporate in isolation from the bulk of water underneath the ice. The fraction of total water in the pan would thus be reduced without affecting the isotopic composition of the bulk ice. Sublimation of ice at night would add to this effect. A similar effect would be introduced by microdroplet vaporization without isotope fractionation during daytime at strong winds as suggested by Gonfiantini et al. (2020). Applying a 'virtual outlet' introduced by these authors – i.e. a fraction of water that is lost without fractionation – in the isotope mass balance equation yields an excellent fit in all three plots of d-excess, $\delta^{18}O$ and $\delta^{2}H$ vs residual fraction for n = 0.59 ± 0.06 with 20 ±4 % loss of water without fractionation (Fig. 9). The hypothesized loss of water without isotope fractionation – either during thawing, due to sublimation or microdroplet vaporization – would have a negligible effect on isotopic data in a diagram of d-excess over $\delta^{18}O$ (Fig. 6b). At given boundary conditions, the best fit for this purely isotopic correlation is obtained for a value of n = 0.55 ± 0.09, which is within error identical with the turbulence coefficient n = 0.59 ± 0.06 derived from the virtual outlet model.

The disadvantage of the latter model is the requirement of a $\delta^{18}O_V$ value, which in this case is only poorly constrained by a few measurements, which in turn translates into a higher uncertainty. For the above calculation, $\delta^{18}O_V$ = -19.4 ± 3 ‰ was used, as derived from our own vapour measurements carried out during the period of the experiment. The obtained value of n = 0.55 ± 0.09 is in good agreement with the global range of reported turbulence coefficients (Merlivat and Jouzel, 1979; Gonfiantini, 1986; Mathieu and Bariac, 1996; Surma et al., 2018), and thus indirectly supports the accuracy of the measured $\delta^{18}O_V$ value.

In a diagram of ^{17}O-excess vs $\delta^{18}O$, the isotopic data fall below the predicted evaporation trend, regardless which model or turbulence coefficient is used (Fig. 6a). This mismatch may be caused by two effects: 1) Partial melting during the thawing of our experiment in the morning may result in uncontrollable mixing effects that are only observable in a ^{17}O-excess over $\delta^{18}O$ diagram (Fig. S5); 2) Diurnal variations of temperature and relative humidity, generate corresponding changes of the theoretical isotopic end point of evaporation leading to a diurnal evolution of the simple evaporation trajectory (Fig. S6; Surma et al., 2018). Both effects become increasingly important, as the experiment progresses to smaller residual water volumes, consistent with our data. High-resolution sampling of similar evaporation experiments may aid in resolving these two effects in the future.

hat verschoben (Einfügung) [10]

hat verschoben (Einfügung) [9]

hat gelöscht: ^{17}O-excess vs $\delta^{18}O$

hat gelöscht: . In this case,

hat gelöscht: unresolvable effects may be the reason for the mismatch.

hat gelöscht: S4). Furthermore, in evaporation experiments the diurnal

hat gelöscht: and

hat gelöscht: lead

hat gelöscht: (pan) evaporation trajectory (Fig. S5; Surma et al., 2018)

hat gelöscht: Unfortunately, we were not able to perform the necessary high…

hat gelöscht: the

hat gelöscht: experiment to fully resolve

hat gelöscht: and obtain the most accurate average evaporation trajectory.

In conclusion of this experiment, we suggest that the complementary analysis of all water isotopes in an evaporation experiment principally allows the determination of the turbulence coefficient. The effect freezing and thawing on the total water loss was not fully resolvable from our experimental data. Hence, we used the turbulence coefficient of $n = 0.55$ for the following modelling calculations, which was derived from the isotopic correlation between d-excess and $\delta^{18}O$, independently from the fraction of remaining water.

6. Discussion: Isotopic hydrology in the Salar del Huasco Basin

6.1 Mixing in tributaries and groundwater aquifers in the Salar del Huasco basin

The Collacagua river and its tributaries originate from springs at different altitudes in the Salar del Huasco basin (c.f. Fig. 1) and could be expected to comprise a somewhat lower $\delta^{2}H$ and $\delta^{18}O$ composition than evaporated salar water due to the altitude effect (Uribe et al., 2015). Samples from the Collacagua river fall below the GMWL, reflecting a significant evaporation history. Likewise, the $\delta^{18}O$ values of springs in the Salar del Huasco basin are slightly higher than local precipitation ($\delta^{18}O$ = -17 to -13 ‰; Scheihing et al., 2017 and references therein), and the d-excess as well as ^{17}O-excess generally fall below the LMWL/GMWL (Fig. 10). This is a common observation for groundwater in the Atacama Desert and other desert environments (Aravena, 1995; Surma et al., 2015, 2018). Based on diagrams of d-excess over $\delta^{18}O$, this offset has been attributed to evaporation of precipitation during infiltration into the soil in previous studies (Aravena, 1995; Fig. 10b). However, all spring and river samples fall below any reasonable evaporation trend in triple oxygen isotope space (Fig. 10a). As such, evaporation along the river path or within the aquifer cannot be solely responsible for the observed isotopic composition. Additional modification of river and groundwater by mixing of different sources must be invoked to explain the triple oxygen isotope composition. Mixing most likely occurs during infiltration into the soil between precipitation and older, evaporated connate water in the vadose zone. Mixing may also take place with water adsorbed onto salts, e. g. halite (NaCl), or structurally bonded water of minerals, e.g. mirabilite ($Na_2SO_4 \cdot 10H_2O$), which we observed frequently during sampling in the Salar del Huasco environment.

6.2 Hydrological processes in the salar

The isotopic composition of lakes and ponds from the Salar del Huasco sampled in the period from 09/17 to 03/19 principally reflects the evaporation trend predicted by the C_xG model for given boundary conditions (Table 3; Fig. 4). Most of the ponds fall on the recharge evaporation trajectory indicating that evaporation occurs while recharge takes place by surface inflow from springs, streams and creeks as well as groundwater recharge dominate the hydrological system. Ponds with high $\delta^{18}O$ values sampled in the southern/south-western area of the salar in 09/17 and 09/18 fall within the envelope spanned by the trajectories for recharge evaporation and simple evaporation at the same boundary conditions (Fig. 4a, c). These ponds may have been isolated from recharge a short time before sampling due to the general lowering of the water table during the dry season and

hat gelöscht: experiments
hat gelöscht: to determine
hat gelöscht: to constrain the isotopic composition of ambient vapour with sufficient confidence. The remaining uncertainty in
hat gelöscht: accuracy of
hat gelöscht: estimate
hat formatiert: Schriftart: Nicht Kursiv
hat gelöscht: in this particular study is, fortunately, not relevant
hat gelöscht: discussion
hat gelöscht: **6.3 Springs and the Collacagua river**¶ The different aquifers in the Salar del Huasco basin are reasonably similar in isotopic composition as indicated by previously published isotopic data of springs and wells (-12.56 ± 1.36 ‰ in $\delta^{18}O$ and 3.2 ± 5.7 ‰ in d-excess; data from Fritz et al., 1981; Uribe et al., 2015; Jayne et al., 2016). These values are in good agreement with our own data derived from springs sampled in 09/17 around the salar with average $\delta^{18}O$ of -12.45 ± 0.64 ‰, d-excess of 2.2 ± 2.9 ‰, and ^{17}O-excess of 11 ± 7 per meg. The springs' isotopic composition shows only slight intra- and interannual variability comprising average $\delta^{18}O$, d-excess and ^{17}O-excess values of -12.31 ± 0.50 ‰, 1.3 ± 2.2 ‰ and 6 ± 7 per meg in 09/18 and -12.55 ± 0.68 ‰, 5.5 ± 2.0 ‰, and 2 ± 6 per meg in 03/19, respectively. The $\delta^{18}O$ values of springs in the Salar del Huasco basin are within the range of local precipitation ($\delta^{18}O$ = -17 to -13 ‰; Scheihing et al., 2017 and references therein), but the springs' isotopic range generally falls below the GMWL. This seems to be typical for groundwater in the Atacama Desert and other desert environments (Aravena, 1995; Surma et al., 2015, 2018) and may be attributed to evaporation of precipitation during infiltration into the soil (Aravena, 1995). The isotopic compositions of springs from the Salar del Huasco basin [11]
hat nach unten verschoben [11]: halite (NaCl), or structurally bonded water of minerals, e.g.
hat gelöscht: mirabilite ($Na_2SO_4 \cdot 10H_2O$), which were commonly observed in the Salar del Huasco environment.¶ ... [12]
hat nach oben verschoben [8]: (Uribe et al., 2015).
hat verschoben (Einfügung) [11]
hat gelöscht: The measured isotopic composition of the Collacagua river likely reflects a mixture of water from its tributaries ... [13]
hat gelöscht: reflect
hat gelöscht: trends
hat gelöscht: –
hat gelöscht: 2
hat gelöscht: 9
hat gelöscht: close to
hat gelöscht: recharged
hat gelöscht: along with
hat gelöscht: by
hat gelöscht: (Fig. 9). A few ponds sampled in 03/19 seem to be 'non-recharged' as their isotopic composition follows the simple ... [14]

evolved from the recharge evaporation trajectory towards the simple evaporation trajectory without a general change in climatic boundary conditions.

Other, seemingly isolated ponds from the overflow region connecting the *Laguna Jasure* with the northern subsystem, sampled in 03/19, clearly fall on the simple evaporation trajectory (Fig. 4e). These ponds were probably remnants of a major flooding in the previous austral summer and cut off from recharge for long enough prior to sampling to evolve all the way from the recharge evaporation trajectory or a mixing curve (see below) to the simple evaporation trajectory. In general, both evaporation trends – recharge evaporation and simple evaporation – are well resolved in the plot of ^{17}O-excess over δ^{18}O (Fig. 4a, c, e) but are indistinguishable in a diagram of d-excess over δ^{18}O (Fig. 4b, d, f).

Ponds sampled in 09/17 in the northern and eastern part of the salar fall generally below the predicted recharge evaporation trajectory (Fig. 4a), but instead within the envelope for mixing defined by the inflow and terminal lake endmembers. Thus, in addition to evaporation and recharge, mixing of younger, less evaporated floodwater and older, more evaporated lake water is at least of temporary importance. At the Salar del Huasco, the seasonality of precipitation and the impact of evaporation cause fluctuations in the groundwater table and occasional flooding. An increase in the groundwater table after heavy rainfalls or snowmelt may lead to admixture of fresh water to the pre-evaporated shallow subsurface flow or pond water. The episodic nature of precipitation should result in rather transient mixing events at the Salar del Huasco. This episodic mixing model differs from the continuous mixing hypothesis proposed by Herwartz et al. (2017) at the Salar de Llamará in the Central Depression of the Atacama Desert, where continuous admixture of isotopically light groundwater to a pre-evaporated subsurface flow may lead to systematic variations in the isotopic composition of inflowing water along the flow path.

6.3 Isotopic residence time of ponds

The isotopic composition of a pond represents an integrated signal over the residence time of the isotopes in the pond. This residence time is specific for each pond and depends on its surface-to-volume ratio, recharge, and the evaporation rate. Only very small water volumes may capture diurnal variations as shown in pan evaporation experiments (Surma et al., 2018). In contrast, deeper water bodies integrate over longer time intervals. Diurnal cycles and changing conditions over several days or weeks will be smoothed out, particularly if local conditions, e.g. a rough wind regime, favour a well-mixed lake. The residence time may be approximated considering the turnover rate of ponds. For a terminal lake, the turnover rate (TR) equals the vaporization rate (φ_{vap}), which is a function of the potential evaporation (E_{pot}) and relative humidity (h): $TR_{E/I=1} = \varphi_{vap} = E_{pot}/(1\text{-}h)$ (Gonfiantini et al., 2018). Mean annual potential evaporation at the Salar del Huasco of about 2290 mm (DGA, 1987) together with the mean annual relative humidity of 40 % results in a mean turnover rate of 318 mm/month (11 mm/d). As isotopic steady-state conditions are reached asymptotically, the residence time is better approximated by the isotopic 'half-turnover-time': $t_{1/2} = \ln(2)/(d \cdot TR)$, with *d* denoting the depth of the water body. Ponds in the Salar del Huasco are very shallow with depths typically < 30 cm resulting in an isotopic half-turnover-time of < 20 days. Considering seasonal variability of the potential evaporation rates and relative humidity (150 mm/month and 33% in austral winter, 200 mm/month and 54 % in austral summer; DGA, 1987; CEAZA, 2020), the isotopic half-turnover-time varies

hat gelöscht: A considerable number of ponds, particularly those sampled in 09/17, falls below the predicted recharge evaporation trajectory (Fig. 9). This offset may be attributed to uncertainty in the model input parameters (δ_{WI}, δ_V, *T*, *h*, *n*) but can also be related to mixing processes. Both effects are examined in the following.¶

6.4.1 Model uncertainty¶

The model input parameters include (1) the isotopic composition of inflowing water (δ_{WI}), which was inferred from the measured isotopic composition of local springs, (2) the isotopic composition of atmospheric vapour (δ_V) estimated from a two-spot measurement, (3) relative humidity (*h*) and temperature (*T*), for which mean seasonal daytime conditions were considered, and (4) the turbulence coefficient (*n*), which was derived from pan evaporation experiments. As previously shown, changes in relative humidity, temperature, and the turbulence coefficient have only a minor impact on evaporation trajectories in triple oxygen isotope space for the given boundary conditions at the Salar del Huasco (Fig. 4). Thus, particularly the uncertainty and variability in the isotopic composition of inflowing water and atmospheric vapour may contribute to deviations and scatter of pond data along the predicted recharge evaporation trajectory in the diagram of ^{17}O-excess over δ^{18}O (Fig. 9a).¶

Ponds and lakes in the Salar del Huasco receive inflow from multiple sources that especially differ in their ^{17}O-excess values. The isotopic composition of inflowing water also varies slightly intra- and interannually due to the seasonality of precipitation and the impact of evaporation (Fig. 8). The effect of source variability on the evaporation trajectory is illustrated in the figs. 10a and 10b. In these diagrams, evaporation trajectories were modelled for the whole isotopic range of springs observed in 09/17. The variability in

between 14 and 26 days for a 30 cm deep pond. To account for the above residence time, evaporation trajectories were modelled with temperature and relative humidity values averaged over 10 or 20 days prior to sampling in March and September, respectively (Fig. 4). Diurnal variations in the evaporation rate were accounted for using daytime (6-18 h) values.

6.4 Impact of climatic dynamics

Considerable seasonal and diurnal variability in environmental conditions at the Salar del Huasco impose variations in climatic boundary conditions during the isotopic residence time of a few weeks to a few months. Moreover, the observed mixing of different generations of precipitation during infiltration and possibly longer residence time of water within the aquifers feeding the spring sources of the lakes and ponds in the Salar del Huasco should result in some variability of the starting point of an evaporation trajectory. Consequently, triple oxygen isotope evaporation trajectories of the C-G model are subject to shifts over time. To evaluate the impact of such variability on the C-G model's resolving power of hydrological processes and detection of mixing from model mismatch in particular, different scenarios were simulated within the range of observed source water and climate variability. The following simulations were focussed on our main field campaign in 09/17, where mixing was identified to have affected the isotopic composition of ponds.

The effect of source variability is most visible in a broader range of evaporation trajectories in the diagram of ^{17}O-excess over δ^{18}O for through-flow ponds and lakes with E/I < 0.5 (Fig. 9a). Source variability may account for the offset of many of the ponds, but a number of those with seemingly high E/I ratios fall well below the simulated envelope.

The impact of variability in the ambient isotopic composition of vapour ($\delta^{18}O_V$) that could potentially affect evaporation trajectories in the C-G model, was estimated using the standard deviation (1 SD = 3.3 ‰) of the three direct measurements distributed over the time interval of this study (Fig. 9c-d). Again, many of the ponds are plotting inside the predicted evaporation envelope defined by variability of $\delta^{18}O_V$ except for those ponds with high E/I that again fall outside the range. To explain these ponds with an evaporation trajectory shifted by variability of ambient vapour composition, $\delta^{18}O_V$ values of about -30 ‰ or even lower would be necessary. This seems to be unlikely considering our measurements (-21.0 ± 3.3 ‰). Most importantly, however, the combined $^{2}H/^{1}H$, $^{17}O/^{16}O$ and $^{18}O/^{16}O$ data cannot be reproduced by invoking a very low $\delta^{18}O_V$ value. With an extreme $\delta^{18}O_V$ of about -30 ‰, the evaporation trajectory may be forced through those ponds below the envelope in ^{17}O-excess, but that would result in an evaporation trajectory falling well above the majority of ponds in the diagram of d-excess over δ^{18}O (Fig. 9c-d). The model outcome is very well constrained in terms of variability in $\delta^{18}O_V$ because trends move in opposite directions between the two plots.

Sensitivity tests suggest a low impact of seasonal and diurnal variability in relative humidity, temperature, and wind conditions on the isotopic composition of lakes and ponds in the Salar del Huasco (Fig. S4). To verify this, we compared recharge evaporation trajectories for daily mean (0-24h; h = 33 %, T = 4°C) and daytime mean conditions (6-18 h; h = 27 %, T = 7 %). Additionally, we modelled the recharge evaporation trajectory for daily mean relative humidity and temperature (h = 20 %, T = 10°C) weighted for the mean diurnal distribution of temperature and wind speed. High temperature and high wind speed amplify evaporation and were thus stronger weighted. Evaporation trajectories of all three scenarios fall close to each other in

hat gelöscht: spring water, particularly in $^{17}O\text{-excess}_{WI}$, broadens the range of evaporation trend lines in the diagram of ^{17}O-excess over δ^{18}O, especially for through-flow lakes (E/I < 0.5). As demonstrated in fig. 10, source variability can account for the offset of most of the ponds. However, a few ponds with apparently high E/I ratios still fall below the predicted envelope (Fig. 10a, b).¶
The value of $\delta^{18}O_V$ was estimated from a two-spot measurement but the isotopic composition of atmospheric vapour might be more variable over the course of the year. Assuming an uncertainty of 5 ‰ in $\delta^{18}O_V$, the isotopic composition of ponds plotting close to the predicted evaporation trend can be covered (Fig 10c). However, $\delta^{18}O_V$ values of about -30 ‰ or even lower would be necessary to fit the isotopic data with the largest offset (Fig. 10c). This seems to be unlikely considering our measurements (-19.4 ‰). Furthermore, using $\delta^{18}O_V$ = -30.0 ‰, all pond data would fall slightly above the predicted evaporation trajectory in a diagram of d-excess over δ^{18}O (Fig. 10d).¶
Sensitivity tests suggests that the impact of large seasonal and diurnal variability in relative humidity, temperature, and wind conditions on the isotopic composition of

hat gelöscht: is low

hat gelöscht: 4

hat gelöscht: assumption

hat gelöscht: annual

hat gelöscht: (h = 33 %, T = 8°C) and

hat gelöscht: seasonal daytime

hat gelöscht: 6

hat gelöscht: 23 %) (Fig. 10e, f).

hat gelöscht: trajectories

hat gelöscht: seasonal

hat gelöscht: 17

hat gelöscht: 9

hat gelöscht: (Fig. 10e, f).

hat gelöscht: All three evaporation

triple oxygen isotope space (Fig. 9e), demonstrating that variability in relative humidity and temperature cannot account for the larger deviations of ponds from the recharge evaporation trajectory in the triple oxygen isotope plot that we attributed to either mixing or cut-off from recharge and evolution along a simple evaporation trajectory.

Collectively, these sensitivity analyses support our conclusion of mixing with flood water. Flooding in this case does not necessarily invoke inundation originating from the springs and inflow channels along the salar's margin, but may as well be the result of a rising groundwater table, which will mostly affect the more central, low-lying ponds that are also more evaporated. In fact, samples that indicate mixing all show advanced evaporation, i.e. plot rather to the right in the diagram. These results demonstrate the capability of the ^{17}O-excess parameter to resolve mixing processes. In contrast, the d-excess parameter cannot distinguish mixing from evaporation at variable climatic boundary conditions at the Salar del Huasco (Fig. 11f).

7 Conclusion

When applied to the triple oxygen isotope system, the classic Craig-Gordon isotope evaporation model reliably predicts the recharge evaporation trend of through-flow ponds within the Salar del Huasco, N-Chile, at ambient climatic boundary conditions and thus, by inference, from any lacustrine system in general. A requirement for that is an on-site estimate of the wind turbulence coefficient of the C-G model. Although the turbulence coefficient has been suggested to cause deviation from the C-G model due to additional kinetic effects at high wind speed (Gonfiantini et al. 2020), our on-site experiment suggests that this exponent may be nonetheless reasonably estimated by the C-G model from pan evaporation experiments using the relationship between d-excess and $\delta^{18}O$. The effects of hydrologic dynamics within a groundwater-recharged lacustrine system on the accuracy of the C-G model are demonstrable in this case study of a lake from an extremely arid and climatically very dynamic environment. Cut-off from recharge during drought is visibly detectable in triple oxygen isotope data. Likewise, flooding, i.e. the rapid mixing of evaporated water from the lake with fresh flood water of a different isotopic composition, can also be identified using triple oxygen isotope data. In the classic δ^2H–$\delta^{18}O$ system, the evaporation trajectories as well as mixing curves fall on top of each other. Therefore, these processes are not resolvable with conventional δ^2H–$\delta^{18}O$ measurements and the variable defining the hydrologic balance of a lake – i.e. the evaporation-to-inflow ratio (E/I) – cannot be determined unambiguously by the C-G model using the classic δ^2H-$\delta^{18}O$ system alone. The C-G model – and thus, the critical E/I variable – is well constrained when using all three isotope ratios – $^2H/^1H$, $^{17}O/^{16}O$ and $^{18}O/^{16}O$ – by the fact that evaporation trajectories move in opposite directions relative to measured data in the respective d-excess and ^{17}O-excess plots when input variables change. Triple oxygen isotope data are also capable of identifying mixing of precipitation with older, pre-evaporated connate water during infiltration in a groundwater recharge area. By combining the advantages of triple oxygen isotope data in terms of resolving fundamental hydrological processes – specifically mixing and the different types of evaporation with and without recharge – with the advantage of the classic δ^2H-$\delta^{18}O$ system regarding the estimation of the

hat gelöscht: 10e)

hat gelöscht: . However, the modelled evaporation trajectories cover the whole isotopic range of ponds in the diagram of d-excess over $\delta^{18}O$ (Fig. 10f). Thus, diurnal and seasonal variations in relative humidity, temperature and also wind conditions may contribute

hat gelöscht: the variability of isotopic data along the

hat gelöscht: trend line in the plot of d-excess over $\delta^{18}O$

hat gelöscht: **6.4.2 Mixing within the Salar**¶
The overall uncertainty of model input parameters cannot fully explain the offset of ponds from the predicted recharge evaporation trajectory (Fig. 10). This holds especially for ponds with E/I > 0.5, which are apparently common in the northern area of the salar (Fig. 9a). For these ponds, mixing is certainly an important process.¶
All ponds and lakes fall within the envelope for mixing defined by the mixing line for a terminal lake (Fig. 9). At the Salar del Huasco, mixing may occur episodically due to fluctuations in the groundwater table that are associated with the seasonality of precipitation and the impact of evaporation. After heavy rainfalls or snowmelt, the groundwater table rises leading to admixture of fresh water to the pre-evaporated shallow subsurface flow or pond water. Mixing is most significant for highly evaporated ponds that isotopically strongly differ from groundwater. Mixing due to episodic flooding occurs only occasionally and, thus, the effect on ponds' isotope composition should be of transient nature. After the mixing event, the isotopic composition of the pond water may tend to re-establish steady-state conditions on the recharge evaporation trajectory. As proposed by Herwartz et al. (2017), mixing processes can also occur continuously by admixture of isotopically light groundwater to a pre-evaporated subsurface flow, leading to variations in the isotopic composition of inflowing water for individual ponds. Continuous mixing may also affect ponds at the Salar del Huasco, additionally to the episodic mixing component.¶
Besides mixing processes, fluctuations in the groundwater table can lead to changes in the recharge rate, increasing the E/I ratio with decreasing water level. Drop down of the water table over the course of the year may ultimately lead to isolation from recharge for individual ponds. When recharge is completely stopped, the isotopic composition of the lake evolves from the recharge evaporation trajectory towards the simple evaporation trajectory. This is particularly observed in the southern area of the salar, where ponds span a wide range in isotopic composition falling within the envelope spanned by predicted trajectories for recharge and simple (pan) evaporation (Fig. 9).¶

hat gelöscht: The classic Craig-Gordon isotopic evaporation model reliably predicts isotopic evaporation trends of lakes and ponds in highly dynamic lacustrine systems in a desert environment with considerable seasonal and diurnal variability in temperature and relative humidity. The Salar del Huasco is dominated by recharge evaporation. Inflow from multiple sources with some spatial and temporal range in isotopic composition cause minor variability in the isotopic evolution of lakes and ponds along the dominant recharge evaporation trajectory. Deviations from this trajectory occur due to episodic flooding after precipitation events that may result in the emergence of ephemeral non-recharged ponds. Additionally, lateral inflow or a rising groundwater table can cause isotopic mixing of pre-flood brines with slightly pre-evaporated floodwater. It may even be possible to identify unknown sources from such mixing trajectories. A rapidly receding groundwater table over a few months after the flood may lead to cut off from recharge for ephemeral ponds at slightly elevated locations. Our results demonstrate that triple oxygen ...[15]

critical wind turbulence exponent, a higher level of accuracy in the hydrologic balance estimate of a lake – or an aquifer – may be achieved when applying the C-G model to lake water isotope data.

Data availability

All data reported herein is provided in the Supplement.

Author Contributions

MS, CV and DH designed the study. CV, MS and CD were responsible for field work. CV conducted data analysis. CV, MS and DH evaluated the data. CV, MS and DH wrote the manuscript with contributions from CD.

Competing Interests

The authors declare that they have no conflict of interest.

Acknowledgements

This work was supported by the German Research Foundation (DFG) [268236062 – SFB 1211, subproject D03]. We thank Franc Megušar and Le-Tehnika (Kranj, Slovenia) for producing the Stirling cooler cycle system. Further, we thank the two anonymous reviewers whose constructive comments significantly improved the manuscript.

References

Acosta, O., Custodio, E., 2008. Impactos ambientales de las extracciones de agua subterránea en el Salar del Huasco (norte de Chile). Bol. Geol. y Min. 119, 33–50.

Alexandre, A., Landais, A., Vallet-Coulomb, C., Piel, C., Devidal, S., Pauchet, S., Sonzogni, C., Couapel, M., Pasturel, M., Cornuault, P., Xin, J., Mazur, J.-C., Prié, F., Bentaleb, I., Webb, E., Chalié, F., Roy, J., 2018. The triple oxygen isotope composition of phytoliths as a proxy of continental atmospheric humidity: insights from climate chamber and climate transect calibrations. Biogeosciences 15, 3223–3241. https://doi.org/10.5194/bg-15-3223-2018

Alexandre, A., Webb, E., Landais, A., Piel, C., Devidal, S., Sonzogni, C., Couapel, M., Mazur, J., Pierre, M., Prié, F., Vallet-coulomb, C., Outrequin, C., Roy, J., 2019. Effects of leaf length and development stage on the triple oxygen isotope signature of grass leaf water and phytoliths: insights for a proxy of continental atmospheric humidity. Biogeosciences 16, 4613–4625. https://doi.org/10.5194/bg-16-4613-2019

Angert, A., Cappa, C.D., DePaolo, D.J., 2004. Kinetic ^{17}O effects in the hydrologic cycle: Indirect evidence and implications.

hat gelöscht: further

hat formatiert: Englisch (Vereinigtes Königreich)

hat formatiert: Englisch (USA)

hat formatiert: Französisch

hat formatiert: Englisch (USA)

hat formatiert: Englisch (USA)

hat formatiert: Französisch

hat formatiert: Englisch (USA)

Geochim. Cosmochim. Acta 68, 3487–3495. https://doi.org/10.1016/j.gca.2004.02.010

Aravena, R., 1995. Isotope hydrology and geochemistry of northern Chile groundwaters. Bull. l'Institut Fr. d'études Andin. 24, 495–503.

Aravena, R., Suzuki, O., Peña, H., Pollastri, A., Fuenzalida, H., Grilli, A., 1999. Isotopic composition and origin of the precipitation in Northern Chile. Appl. Geochemistry 14, 411–422. https://doi.org/10.1016/S0883-2927(98)00067-5

Barkan, E., Luz, B., 2005. High precision measurements of $^{17}O/^{16}O$ and $^{18}O/^{16}O$ ratios in H_2O. Rapid Commun. Mass Spectrom. 19, 3737–3742. https://doi.org/10.1002/rcm.2250

Barkan, E., Luz, B., 2007. Diffusivity fractionations of $H_2^{16}O/H_2^{17}O$ and $H_2^{16}O/H_2^{18}O$ in air and their implications for isotope hydrology. Rapid Commun. Mass Spectrom. 21, 2999–3005. https://doi.org/10.1002/rcm.3180

Boschetti, T., Cifuentes, J., Iacumin, P., Selmo, E., 2019. Local meteoric water line of northern Chile (18°S-30°S): An application of error-in-variables regression to the oxygen and hydrogen stable isotope ratio of precipitation. Water 11, 1–16. https://doi.org/10.3390/w11040791

Bowen, G.J., 2020. The Online Isotopes in Precipitation Calculator., version 3.1. http://www.waterisotopes.org

Bowen, G.J., Wassenaar, L.I., Hobson, K.A., 2005. Global application of stable hydrogen and oxygen isotopes to wildlife forensics. Oecologia 143, 337–348. https://doi.org/10.1007/s00442-004-1813-y

Cao, X., Liu, Y., 2011. Equilibrium mass-dependent fractionation relationships for triple oxygen isotopes. Geochim. Cosmochim. Acta 75, 7435–7445. https://doi.org/10.1016/j.gca.2011.09.048

CEAZA, (Centro de Estudios Avanzados en Zonas Áridas), 2020. Estación Salar de Huasco. http://www.ceazamet.cl

Clark, I., Fritz, P., 1997. Environmental Isotopes in Hydrogeology. Lewis Publishers, New York.

Craig, H., Gordon, L.I., 1965. Deuterium and oxygen 18 variations in the ocean and the marine atmosphere, in: Stable Isotopes in Oceanographic Studies and Paleotemperatures. pp. 9–130.

Criss, R.E., 1999. Principles of Stable Isotope Distribution. Oxford University Press.

DGA, 1987. Balance Hídrico de Chile. Santiago, Chile.

Dongmann, G., Nürnberg, H.W., Förstel, H., Wagener, K., 1974. On the enrichment of $H_2^{18}O$ in the leaves of transpiring plants. Radiat. Environ. Biophys. 11, 41–52. https://doi.org/10.1007/BF01323099

Evans, N.P., Bauska, T.K., Gázquez, F., Brenner, M., Curtis, J.H., Hodell, D.A., 2018. Quantification of drought during the collapse of the classic Maya civilization. Science 501, 498–501.

Fritz, P., Suzuki, O., Silva, C., Salati, E., 1981. Isotope hydrology of groundwaters in the Pampa del Tamarugal, Chile. J. Hydrol. 53, 161–184. https://doi.org/10.1016/0022-1694(81)90043-3

Garreaud, R., Vuille, M., Clement, A.C., 2003. The climate of the Altiplano: Observed current conditions and mechanisms of past changes. Palaeogeogr. Palaeoclimatol. Palaeoecol. 194, 5–22. https://doi.org/10.1016/S0031-0182(03)00269-4

Garreaud, R.D., Aceituno, P., 2001. Interannual Rainfall Variability over the South American Altiplano. J. Clim. 14, 2779–2789. https://doi.org/10.1175/1520-0442(2001)014<2779:IRVOTS>2.0.CO;2

Gat, J.R., Bowser, C., 1991. The heavy isotope enrichment of water in coupled evaporative systems, in: Taylor, H.P., O'Neil,

hat formatiert: Französisch

hat formatiert: Englisch (USA)

hat gelöscht: Baker, L., Franchi, I.A., Maynard, J., Wright, I.P., Pillinger, C.T., 2002. A Technique for the Determination of $^{18}O/^{16}O$ and $^{17}O/^{16}O$ Isotopic Ratios in Water from Small Liquid and Solid Samples. Anal. Chem. 74, 1665–1673. https://doi.org/10.1021/ac010509s¶

hat formatiert: Englisch (USA)

hat formatiert: Englisch (USA)

hat formatiert: Französisch

hat gelöscht: 2019

hat formatiert: Französisch

hat gelöscht: [WWW Document]. URL

hat formatiert: Französisch

hat gelöscht: (accessed 11.6.18).

hat formatiert: Englisch (USA)

hat formatiert: Englisch (USA)

hat gelöscht: -sánchez

hat formatiert: Englisch (USA)

hat gelöscht: (80-.).

hat formatiert: Englisch (USA)

hat formatiert: Englisch (USA)

J.R., Kaplan, I.R. (Eds.), Stable Isotope Geochemistry: A Tribute to Samuel Epstein. The Geochemical Society, pp. 159–168.

Gázquez, F., Morellón, M., Bauska, T., Herwartz, D., Surma, J., Moreno, A., Staubwasser, M., Valero-Garcés, B., Delgado-Huertas, A., Hodell, D.A., 2018. Triple oxygen and hydrogen isotopes of gypsum hydration water for quantitative paleo-humidity reconstruction. Earth Planet. Sci. Lett. 481, 177–188. https://doi.org/10.1016/j.epsl.2017.10.020

Gonfiantini, R., 1986. Environmental isotopes in lake studies, in: Fontes, D., Fritz, P. (Eds.), Handbook of Environmental Isotope Geochemistry. Elsevier Science, pp. 119–168.

Gonfiantini, R., Wassenaar, L.I., Araguas-araguas, L., Aggarwal, P.K., 2018. A unified Craig-Gordon isotope model of stable hydrogen and oxygen isotope fractionation during fresh or saltwater evaporation. Geochim. Cosmochim. Acta 235, 224–236. https://doi.org/10.1016/j.gca.2018.05.020

Gonfiantini, R., Wassenaar, L.I., Araguas-Araguas, L.J., 2020. Stable isotope fractionations in the evaporation of water: The wind effect. Hydrol. Process. 34, 3596–3607. https://doi.org/10.1002/hyp.13804

Herwartz, D., Surma, J., Voigt, C., Assonov, S., Staubwasser, M., 2017. Triple oxygen isotope systematics of structurally bonded water in gypsum. Geochim. Cosmochim. Acta 209, 254–266. https://doi.org/10.1016/j.gca.2017.04.026

Horita, J., 1989. Stable isotope fractionation factors of water in hydrated saline mineral-brine systems. Earth Planet. Sci. Lett. 95, 173–179. https://doi.org/10.1016/0012-821X(89)90175-1

Horita, J., 2005. Saline waters, in: Aggarwal, P.K., Gat, J.R., Froehlich, K.F.O. (Eds.), Isotopes in the Water Cycle: , Present and Past Future of a Developing Science. IEA, pp. 271–287.

Horita, J., Cole, D.R., Wesolowski, D.J., 1993. The activity-composition relationship of oxygen and hydrogen isotopes in aqueous salt solutions: II. Vapor-liquid water equilibration of mixed salt solutions from 50 to 100°C and geochemical implications. Geochim. Cosmochim. Acta 57, 4703–4711.

Horita, J., Rozanski, K., Cohen, S., 2008. Isotope effects in the evaporation of water: a status report of the Craig-Gordon model. Isotopes Environ. Health Stud. 44, 23–49. https://doi.org/10.1080/10256010801887174

Houston, J., 2006. Variability of precipitation in the Atacama Desert: Its causes and hydrological impact. Int. J. Climatol. 26, 2181–2198. https://doi.org/10.1002/joc.1359

Jayne, R.S., Pollyea, R.M., Dodd, J.P., Olson, E.J., Swanson, S.K., 2016. Spatial and temporal constraints on regional-scale groundwater flow in the Pampa del Tamarugal Basin, Atacama Desert, Chile. Hydrogeol. J. 24, 1921–1937. https://doi.org/10.1007/s10040-016-1454-3

Landais, A., Barkan, E., Luz, B., 2008. Record of $\delta^{18}O$ and ^{17}O-excess in ice from Vostok Antarctica during the last 150,000 years. Geophys. Res. Lett. 35, 1–5. https://doi.org/10.1029/2007GL032096

Landais, A., Barkan, E., Yakir, D., Luz, B., 2006. The triple isotopic composition of oxygen in leaf water. Geochim. Cosmochim. Acta 70, 4105–4115. https://doi.org/10.1016/j.gca.2006.06.1545

Landais, A., Risi, C., Bony, S., Vimeux, F., Descroix, L., Falourd, S., Bouygues, A., 2010. Combined measurements of $^{17}O_{excess}$ and d-excess in African monsoon precipitation: Implications for evaluating convective parameterizations. Earth Planet.

hat formatiert: Englisch (USA)

hat gelöscht: Haese, B., Werner, M., Lohmann, G., 2013. Stable water isotopes in the coupled atmosphere – land surface model ECHAM5-JSBACH. Geosci. Model Dev. 6, 1463–1480. https://doi.org/10.5194/gmd-6-1463-2013¶

hat formatiert: Englisch (USA)

hat formatiert: Englisch (USA)

hat formatiert: Deutsch

hat formatiert: Englisch (USA)

hat formatiert: Deutsch

hat formatiert: Englisch (USA)

hat gelöscht: Li

hat formatiert: Englisch (USA)

hat gelöscht: Levin, N.E., Soderberg, K., Dennis, K.J., Caylor, K.K., 2017. Triple oxygen isotope composition

hat formatiert: Englisch (USA)

hat gelöscht: leaf waters

hat formatiert: Englisch (USA)

hat gelöscht: Mpala, central Kenya.

hat formatiert: Englisch (USA)

Sci. Lett. 298, 104–112. https://doi.org/10.1016/j.epsl.2010.07.033

Mathieu, R., Bariac, T., 1996. A numerical model for the simulation of stable isotope profiles in drying soils. J. Geophys. Res. Atmos. 101, 12685–12696. https://doi.org/10.1029/96JD00223

Merlivat, L., Jouzel, J., 1979. Global climatic interpretation of the deuterium-oxygen 18 relationship for precipitation. J. Geophys. Res. 84, 5029–5033. https://doi.org/10.1029/JC084iC08p05029

Peters, L.I., Yakir, D., 2010. A rapid method for the sampling of atmospheric water vapour for isotopic analysis. Rapid Commun. Mass Spectrom. 24, 103–108. https://doi.org/10.1002/rcm.4359

Risacher, F., Alonso, H., Salazar, C., 2003. The origin of brines and salts in Chilean salars: A hydrochemical review. Earth-Science Rev. 63, 249–293. https://doi.org/10.1016/S0012-8252(03)00037-0

Scheihing, K., Moya, C., Struck, U., Lictevout, E., Tröger, U., 2017. Reassessing Hydrological Processes That Control Stable Isotope Tracers in Groundwater of the Atacama Desert (Northern Chile). Hydrology 5, 1–22. https://doi.org/10.3390/hydrology5010003

Schoenemann, S.W., Schauer, A.J., Steig, E.J., 2013. Measurement of SLAP2 and GISP $\delta^{17}O$ and proposed VSMOW-SLAP normalization for $\delta^{17}O$ and $^{17}O_{excess}$. Rapid Commun. Mass Spectrom. 27, 582–590. https://doi.org/10.1002/rcm.6486

Sofer, Z., Gat, J.R., 1972. Activities and concentrations of oxygen-18 in concentrated aqueous salt solutions: Analytical and geophysical implications. Earth Planet. Sci. Lett. 15, 232–238. https://doi.org/10.1016/0012-821X(72)90168-9

Sofer, Z., Gat, J.R., 1975. The isotope composition of evaporating brines: Effect of the isotopic activity ratio in saline solutions. Earth Planet. Sci. Lett. 26, 179–186. https://doi.org/10.1016/0012-821X(75)90085-0

Stein, A.F., Draxler, R.R., Rolph, G.D., Stunder, B.J.B., Cohen, M.D., Ngan, F., 2015. NOAA's HYSPLIT atmospheric transport and dispersion modeling system. Bull. Am. Meteorol. Soc. 96, 2059–2077. https://doi.org/10.1175/BAMS-D-14-00110.1

Surma, J., Assonov, S., Bolourchi, M.J., Staubwasser, M., 2015. Triple oxygen isotope signatures in evaporated water bodies from the Sistan Oasis, Iran. Geophys. Res. Lett. 42, 8456–8462. https://doi.org/10.1002/2015GL066475

Surma, J., Assonov, S., Herwartz, D., Voigt, C., Staubwasser, M., 2018. The evolution of ^{17}O-excess in surface water of the arid environment during recharge and evaporation. Sci. Rep. 8, 1–10. https://doi.org/10.1038/s41598-018-23151-6

Uribe, J., Muñoz, J.F., Gironás, J., Oyarzún, R., Aguirre, E., Aravena, R., 2015. Assessing groundwater recharge in an Andean closed basin using isotopic characterization and a rainfall-runoff model: Salar del Huasco basin, Chile. Hydrogeol. J. 23, 1535–1551. https://doi.org/10.1007/s10040-016-1383-1

hat gelöscht: 468, 38–50

hat gelöscht: 08.016

hat formatiert: Englisch (USA)

hat gelöscht: 2017.02.015¶
Luz, B., Barkan, E., 2010. Variations of $^{17}O/^{16}O$ and $^{18}O/^{16}O$ in [16]

hat formatiert: Englisch (USA)

hat formatiert: Englisch (USA)

hat gelöscht: Passey, B.H., Ji, H., 2019. Triple oxygen isotope signatures of evaporation in lake waters and carbonates: A case ... [17]

hat formatiert: Englisch (USA)

hat formatiert: Englisch (USA)

hat formatiert: Deutsch

hat formatiert: Englisch (USA)

hat formatiert: Deutsch

hat formatiert: Englisch (USA)

hat formatiert: Englisch (USA)

hat gelöscht: Uemura, R., Barkan, E., Abe, O., Luz, B., 2010. Triple isotope composition of oxygen in atmospheric water vapor ... [18]

hat formatiert: Englisch (USA)

hat formatiert: Deutsch

Formatiert ... [19]

Formatiert ... [20]

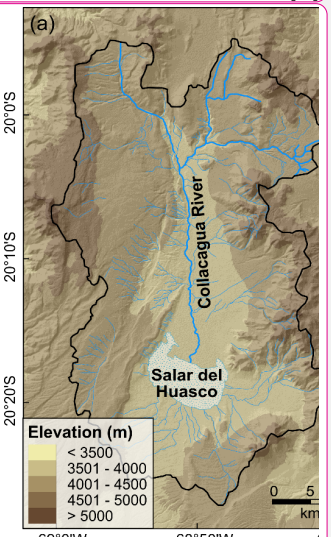

hat gelöscht:

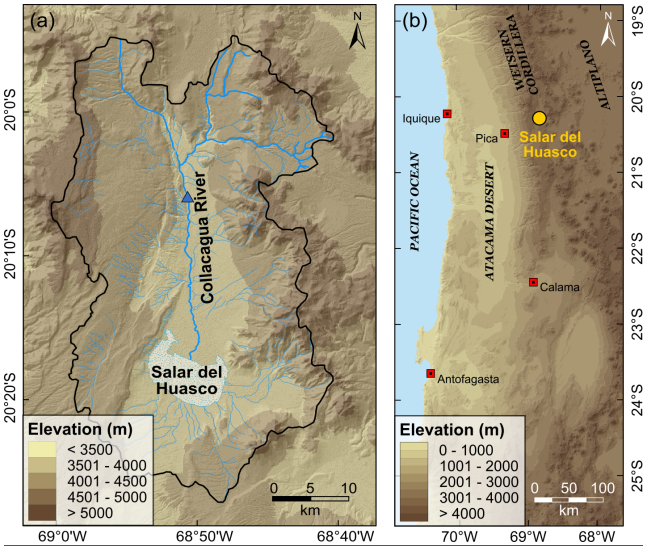

Figure 1: Study Area. (a) Catchment of the Salar del Huasco (Salar del Huasco basin) with drainage. The blue triangle marks the sampling location of the Collacagua river. (b) Overview map. (DEM derived from SRTM data, created using ArcGIS 10.5.1)

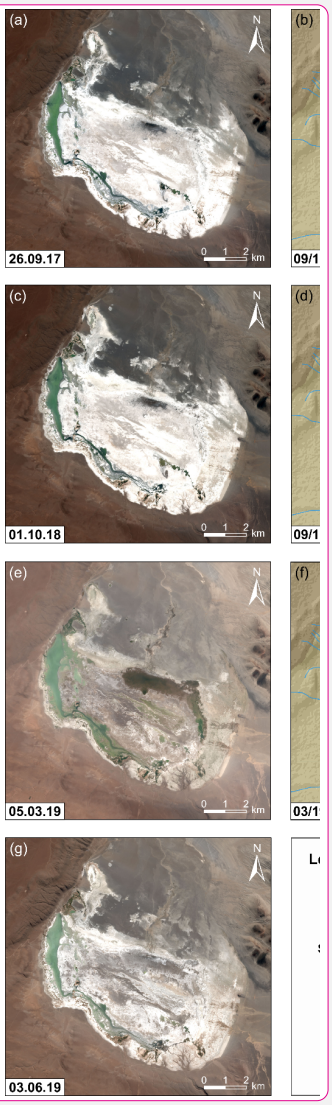

hat gelöscht:

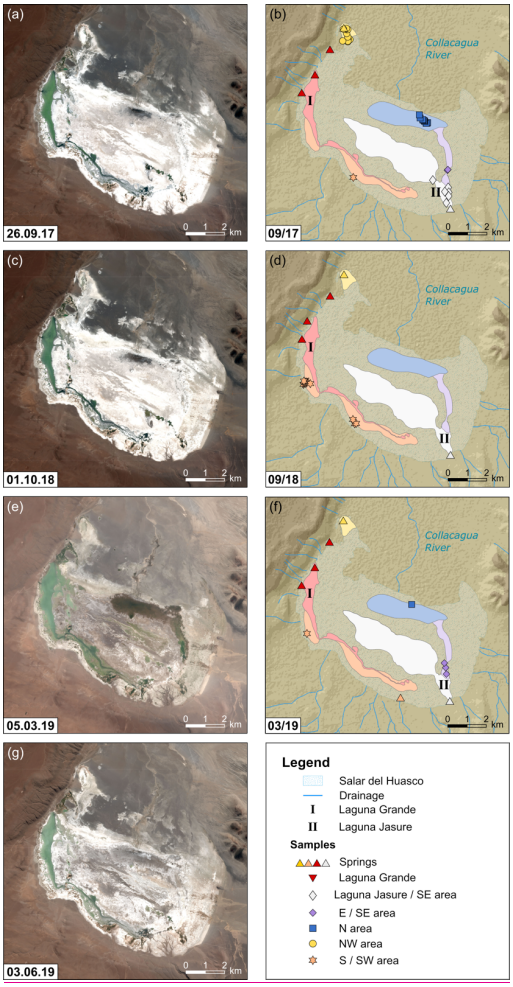

Figure 2: Illustration of the hydrological situation at the Salar del Huasco over the sampling period with sample locations for field campaigns in 09/17 ((a) and (b)), 09/18 ((c) and (d)), and 03/19 ((e) and (f)). Panel (g) reflects the hydrological situation at the Salar del Huasco 6 months after the last sampling campaign. Several hydrological subsystems (coloured areas) were identified based on satellite images (Copernicus Sentinel data, 2017, 2018, 2019) and field observations. Different symbols of sample locations refer to the corresponding hydrological subsystem (see text for details). (DEM derived from SRTM data, created using ArcGIS 10.5.1)

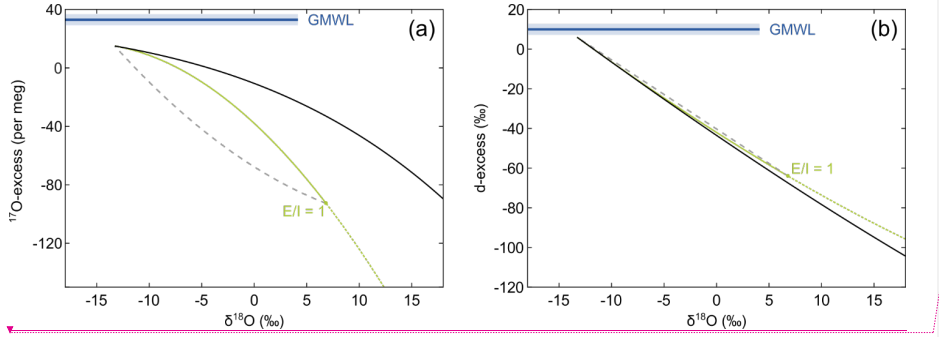

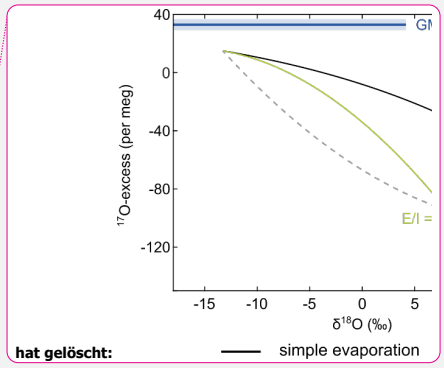

hat gelöscht:

Figure 3: Conceptual comparison of isotope effects associated with the three principal hydrological processes – simple evaporation without recharge, evaporation with recharge, and isotopic mixing – in the diagram of (a) ^{17}O-excess over δ^{18}O and (b) d-excess over δ^{18}O. In the case of simple evaporation, the isotopic composition of an evaporating water body evolves along the black line. Continuous recharge drives the isotopic composition of the evaporating water body below the simple evaporation trajectory onto the green line. The isotopic composition of a recharged lake is determined by the evaporation to inflow (E/I) ratio where increasing E/I lead to higher δ^{18}O and lower ^{17}O-excess values. In the case of a terminal lake (E/I = 1) all inflow is balanced by evaporation. The dashed grey line exemplifies admixture of fresh water similar in isotopic composition to the inflowing water, e.g. flood water, to the evaporated brine of a terminal lake.

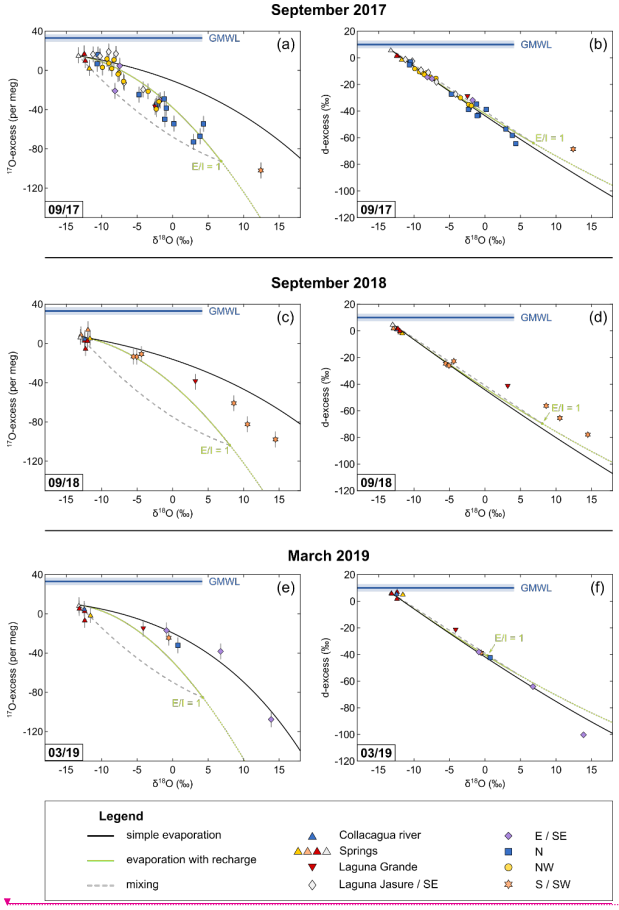

Figure 4: Oxygen and hydrogen isotope data of the Collacagua river, springs, lakes and ponds sampled in the Salar del Huasco basin during field campaigns in 09/17 ((a) and (b)), 09/18 ((c) and (d)), and 03/19 ((e) and (f)). Colour coding refers to different hydrological subsystems (see legend and cf. Fig. 2). Note that the symbol size can be larger than the error bars. Trajectories for simple evaporation (black) and evaporation with recharge (green) were modelled using input parameters as summarized in Table 3. To calculate temperature and relative humidity, daytime (6-18 h) conditions of the 10 (03/19) or 20 (09/17,09/18) prior to sampling were considered (cf. Sect. 6.3). Additionally, admixture of fresh groundwater (dashed grey line) as it might occur during flooding or snowmelt is exemplified for the case of a terminal lake (E/I = 1). The Global Meteoric Water Line (GMWL) serves as reference. Note that the apparent lack of samples on a recharge evaporation trajectory in 09/18 and 03/19 is simply the result of a sampling focus on sources and on ponds cut off from recharge during these campaigns.

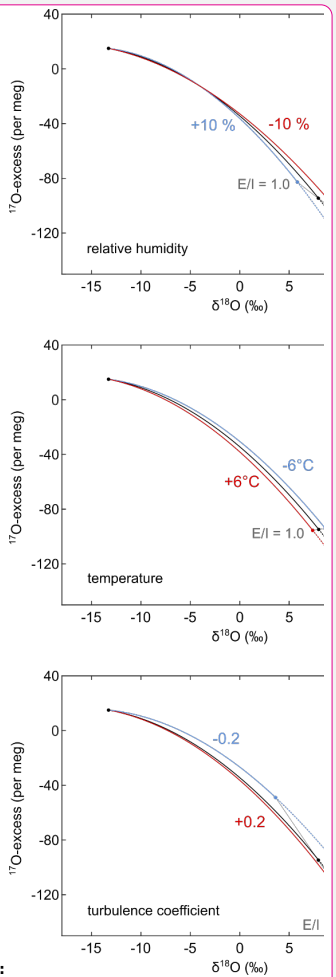

hat gelöscht: Figure 4: Sensitivity of evaporation trajectories in diagrams of ^{17}O-excess over δ^{18}O and d-excess over δ^{18}O to different input parameters for environmental conditions at the Salar del Huasco ... [21]

hat verschoben (Einfügung) [12]

hat verschoben (Einfügung) [13]

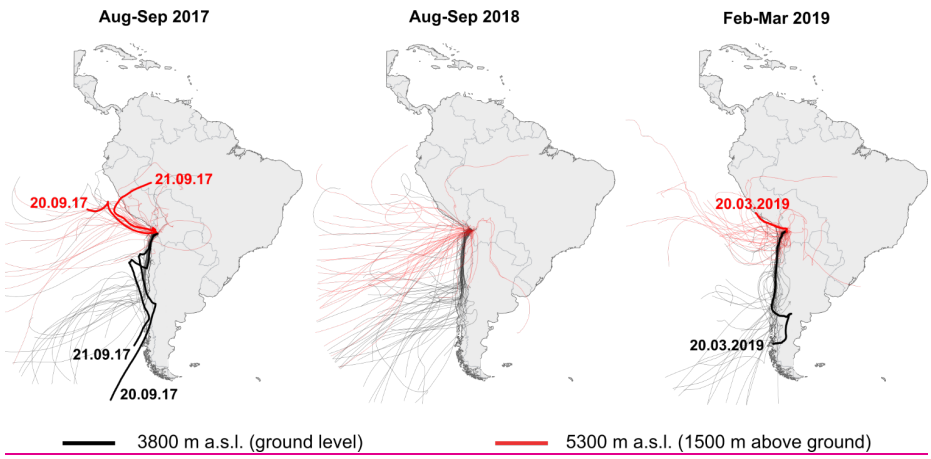

Figure 5: HYSPLIT 7-day air mass back trajectories modelled for ground level at the Salar del Huasco (~3800 m above sea level (a.s.l.)) (black) and 1500 m above ground level (5300 m a.s.l.) (red) in daily resolution for the period from 23.08.2017 to 22.09.2017. The thick red and black trajectories represent modelled back trajectories for the time of vapour sampling on 20.09.17, 21.09.2017 and on 20.03.20

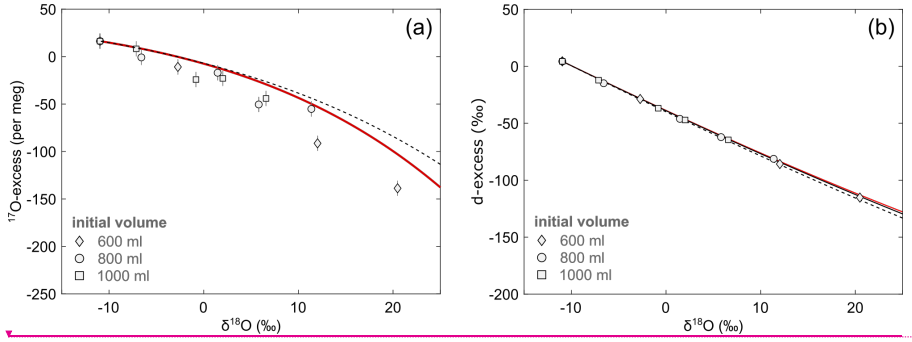

Figure 6: Isotopic data of pan evaporation experiments in the diagrams of (a) ^{17}O-excess over δ^{18}O and (b) d-excess over δ^{18}O. Pan evaporation experiments were carried out with different initial volume of 600 ml (diamonds), 800 ml (circles), 1000 ml (squares). Note that the symbol size can be larger than the error bars. The solid black line in panel (b) shows the best fitting evaporation trajectory (n = 0.55) for the simple evaporation model. The red lines represent the evaporation trajectories modelled using the virtual outlet model with n = 0.59 and an outlet of 20% (see text). Dashed lines illustrate the evaporation trajectories modelled with the simple evaporation model using the same turbulence coefficient as for the virtual outlet model. Model input parameters are summarized in Table 2.

hat gelöscht: the origin of atmospheric air masses at the Salar del Huasco…

hat gelöscht: and

hat gelöscht: .

hat gelöscht: ¶

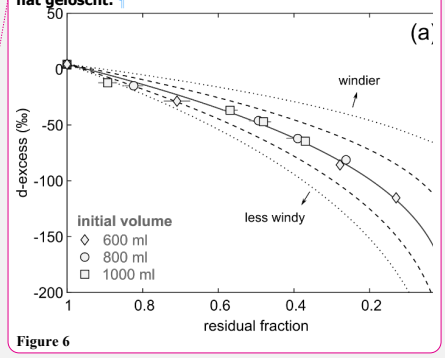

Figure 6

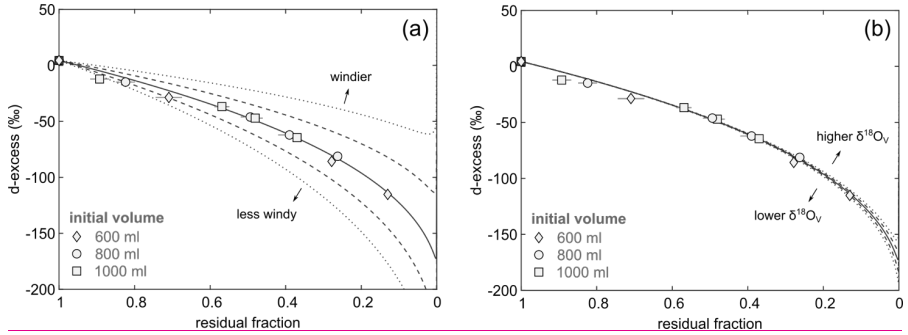

Figure 7: Sensitivity of evaporation trajectories in a plot of d-excess over residual fraction to (a) the turbulence coefficient (*n*) and (b) the isotopic composition of atmospheric vapour ($\delta^{18}O_V$). Isotopic data of pan evaporation experiments with initial volume of 600 ml (diamonds), 800 ml (circles), 1000 ml (squares) are shown for comparison. Note that the symbol size is in most cases larger than the error bars. The solid line represents the modelled evaporation trajectory for simple evaporation using input parameters as summarized in Table 2 and a turbulence coefficient of 0.44. Dashed lines show model results for (a) different turbulence coefficients in intervals of 0.1 and (b) varying $\delta^{18}O_V$ in intervals of 5 ‰, keeping other parameters constant.

hat formatiert: Schriftart: Kursiv

hat formatiert: Schriftart: Kursiv

hat gelöscht: .

hat gelöscht: 1

hat gelöscht: isotopic composition of atmospheric vapour

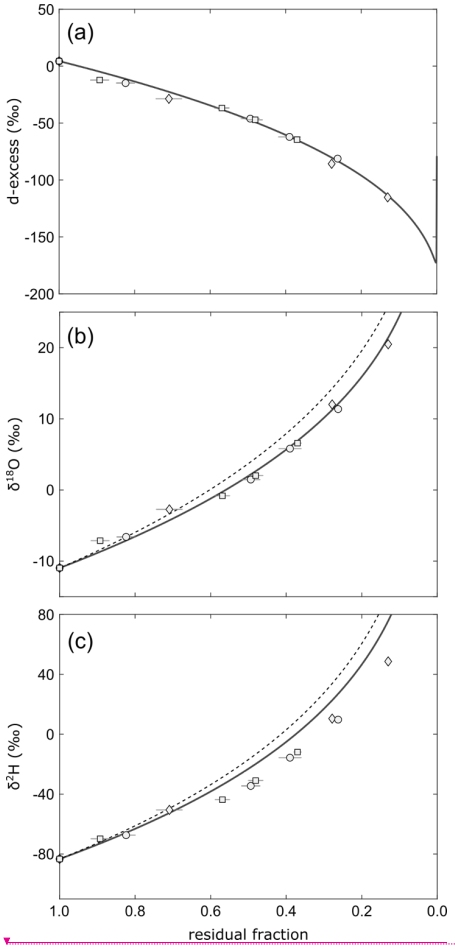

Figure 8: Evolution of (a) $\delta^{18}O$, (b) $\delta^{2}H$, and (c) d-excess of remaining water in the evaporation experiments. The solid lines show evaporation trajectories obtained by fitting the simple evaporation model independently to $\delta^{18}O$ (n= 0.34), $\delta^{2}H$ (n=0) and d-excess (n=0.44) vs residual fraction. Note that the $\delta^{2}H$ data cannot be fitted for any reasonable turbulence coefficient. The dashed lines in (a) and (b) are evaporation trajectories modelled using the same turbulence coefficient as for the d-excess data.

hat gelöscht: ¶

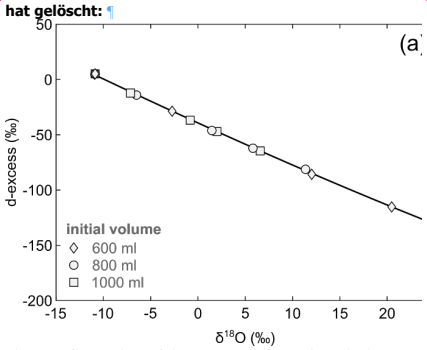

Figure 7: Comparison of simple evaporation trajectories in a diagram of d-excess over $\delta^{18}O$ modelled for (a) n = 0.54 and (b) n = 0.44, keeping other parameters constant (see Table 1). Additionally, isotopic data of pan evaporation experiments with initial volume of 600 ml (diamonds), 800 ml (circles), 1000 ml (squares) are shown. Note that the symbol size is larger than the error bars.¶

¶

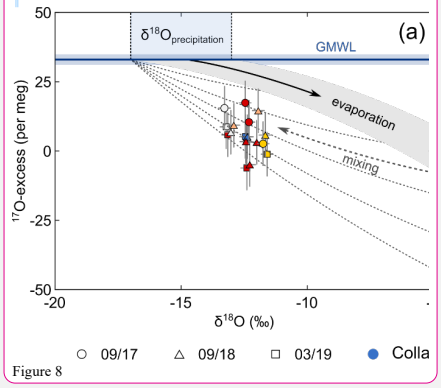

Figure 8

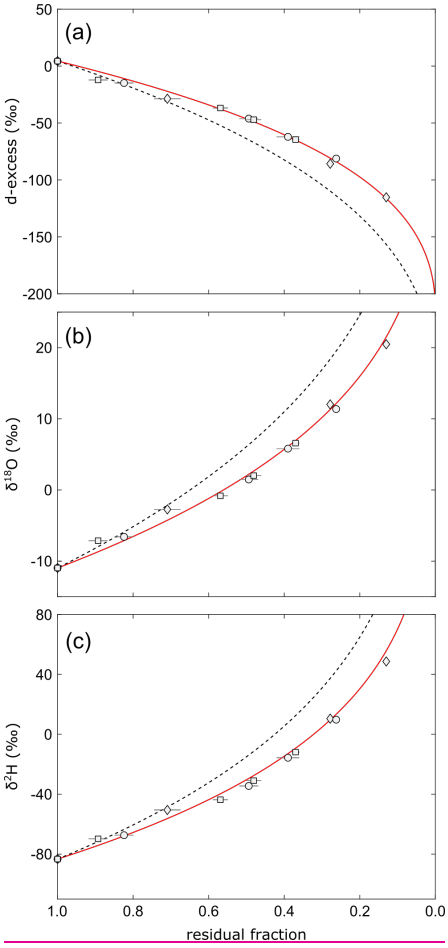

Figure 9: Isotopic evolution of remaining water in evaporation experiments, similar to figure 8. Here, the red lines show evaporation trajectories obtained by fitting the virtual outlet model (n = 0.59, outlet = 20%). The dashed lines represent evaporation trajectories for the simple evaporation model obtained using the same turbulence coefficient as for the virtual outlet model.

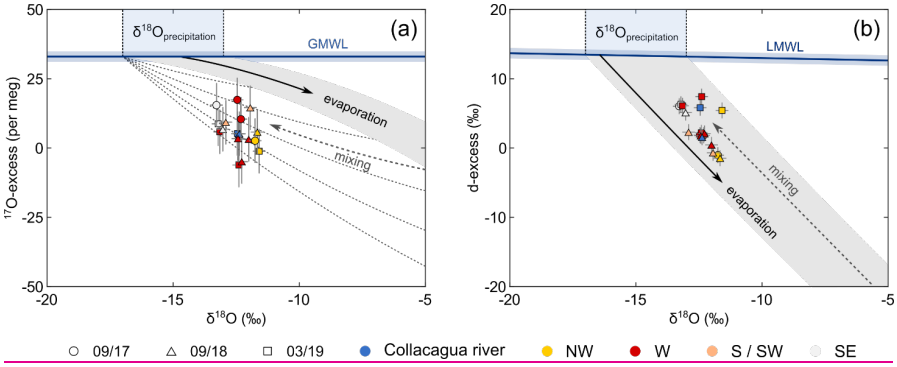

Figure 10: Oxygen (a) and hydrogen (b) isotopic data of the Collacagua river and springs from the Salar del Huasco basin. Colour coding refers to different hydrological subsystems (cf. Fig. 2). The isotopic range of precipitation (-17 to -13 ‰) is derived from previously published data (Scheihing et al., 2017 and references therein). The local meteoric water line (LMWL: $\delta^2H=7.93\cdot\delta^{18}O+12.3$; Boschetti et al., 2019) was derived from precipitation data of northern Chile. Due to the lack of a comprehensive dataset of ^{17}O in precipitation, the global meteoric water line (GMWL) was used as reference in the triple oxygen isotope plot (a). The shaded grey area indicates the isotopic evolution of precipitation undergoing evaporation. The Collacagua river and all local springs fall below the common evaporation trend in a plot of ^{17}O-excess over $\delta^{18}O$ (a). This offset can be explained considering mixing of precipitation with evaporated water in the vadose zone during infiltration into the soil. The effect of mixing is schematically illustrated by the dashed grey lines.

hat formatiert: Hochgestellt

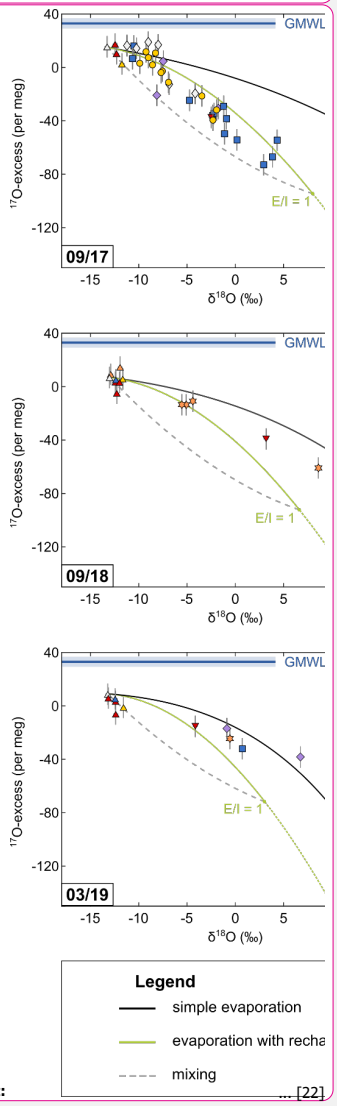

hat gelöscht: ... [22]

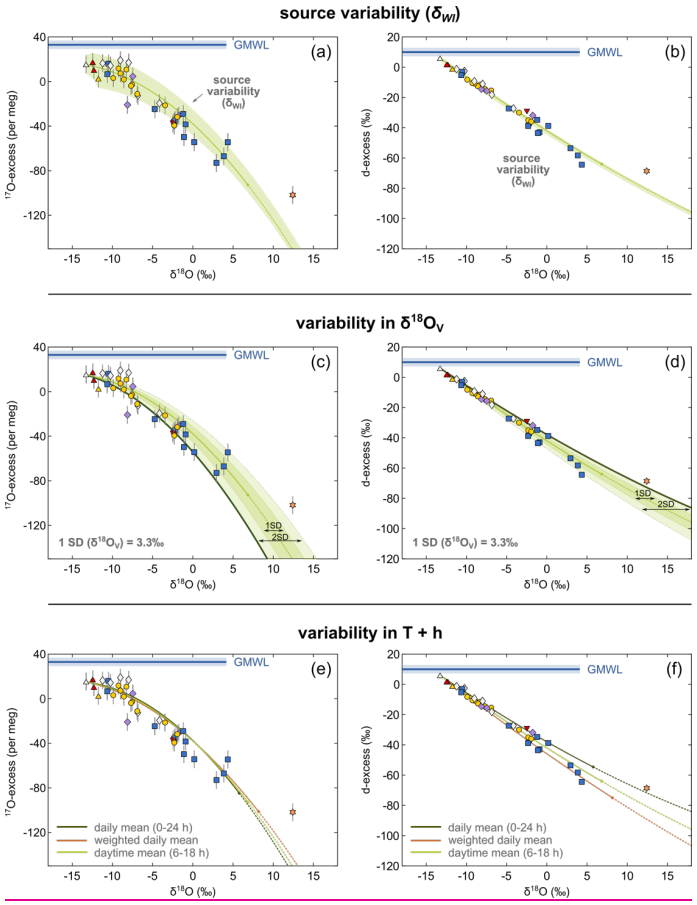

Figure 11: Illustration of the impact of variability and uncertainty in the model input parameters on the evaporation trajectory, exemplified for lakes and ponds sampled in 09/17. The green line shows the modelled recharge evaporation trajectory for mean daytime conditions (6-18 h) at the Salar del Huasco. The shaded green areas in panel (a) and (b) illustrate the uncertainty introduced to the modelled trajectory by spatial variability in the isotopic composition of inflowing water ($\delta^{18}O_{WI}$). The dark solid lines represent corresponding evaporation trajectories in panel (a) and (b). Panel (c) and (d) show the impact of variable $\delta^{18}O_V$ on the evaporation trajectory illustrated by multiples intervals of the SD (1SD = 2.6 ‰; shaded areas). Panel (e) and (f) illustrate the effect of uncertainty in the assumed effective evaporation time interval. Recharge evaporation trajectories have been modelled for (1) daily mean (0-24 h; h = 33 %, T = 4°C) (dark green curve), (2) daily mean h = 20 % and T = 10°C weighted for the average diurnal distribution of temperature and wind speed (brown curve), and (3) daytime mean (6-18 h; h = 27 %, T = 7°C) conditions (light green curve).

hat nach oben verschoben [12]: : Oxygen and hydrogen isotope data of the Collacagua river, springs, lakes and ponds sampled in the Salar del Huasco basin during field campaigns in 09/17 ((a) and (b)), 09/18 ((c) and (d)), and 03/19 ((e) and (f)). Colour coding refers to different hydrological subsystems (see legend and cf. Fig. 2). Note that the symbol size can be larger than the error bars. Trajectories for simple evaporation (black) and evaporation with recharge (green) were modelled using input parameters as summarized in Table

hat gelöscht: 2. Additionally, admixture of fresh groundwater as it might occur during flooding or snowmelt is exemplified for the case of a terminal lake (E/I = 1) (dashed grey line).

hat nach oben verschoben [13]: The Global Meteoric Water Line (GMWL) serves as reference. Note that the apparent lack of samples on a recharge evaporation trajectory in 09/18 and 03/19 is simply the result of a sampling focus on sources and on ponds cut off from recharge during these campaigns.¶

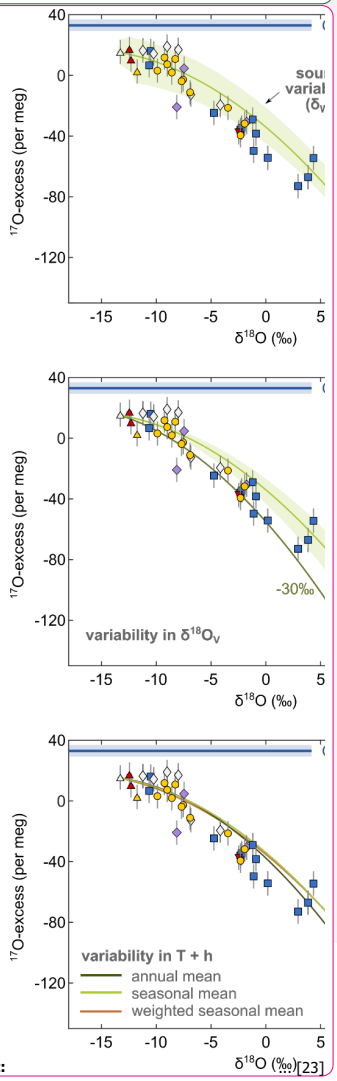

hat gelöscht: [23]

Table 1: Sampling intervals and isotopic data of atmospheric vapour.

Day	Time	$\delta^{17}O$ (‰)	$\delta^{18}O$ (‰)	^{17}O-excess (per meg)	n	$\delta^{2}H$ (‰)	d-excess (‰)	n
20.09.2017	18:30-21:30	-11.1	-21.0	19	2	-136	32	1
21.09.2017	18:30-21:30	-9.4	-17.8	16	2	-114	28	1
mean		**-10.3**	**-19.4**	**18**		**-125**	**30**	
SD		**1.2**	**2.3**	**2.1**		**15**	**2.8**	
20.03.2019	10:00-13:00	-12.9	-24.3	33	2	-154	41	1
overall average		**-11.1**	**-21.0**	**23**		**-135**	**34**	
SD		**1.7**	**3.2**	**9**		**20**	**6**	

Table 2: Model input parameters of the simple evaporation model for pan evaporation experiments. The isotopic composition of initial water and atmospheric vapour was determined by measurement. The effective evaporation time interval was assumed to correspond to the period when T > 0°C to account for the freezing of water in the pans during the night.

Parameter	Value
$\delta^{18}O_{WI}$ (‰)	-10.96
d-excess$_{WI}$ (‰)	4.4
^{17}O-excess$_{WI}$ (per meg)	16
$\delta^{18}O_{V}$ (‰)	-19.4
d-excess$_{V}$ (‰)	30
^{17}O-excess$_{V}$ (per meg)	18
Temperature (°C)	10
Relative humidity (%)	22

hat gelöscht: ¶ ... [24]
hat gelöscht: 1:
hat gelöscht: Relative humidity and temperature were ... [25]
hat formatiert ... [26]
hat gelöscht: experiment. We used mean relative humidity and ... [27]
hat gelöscht: diurnal variability
hat gelöscht: evaporation rate. The turbulence coefficient was ... [28]
hat formatiert ... [29]
Formatiert ... [30]
hat formatiert ... [31]
Formatiert ... [32]
Formatiert ... [33]
hat formatiert ... [34]
Formatiert ... [35]
Formatiert ... [36]
hat formatiert ... [37]
Formatiert ... [38]
Formatiert ... [39]
hat formatiert ... [40]
Formatiert ... [41]
Formatiert ... [42]
hat formatiert ... [43]
Formatiert ... [44]
Formatiert ... [45]
hat formatiert ... [46]
Formatiert ... [47]
Formatiert ... [48]
hat formatiert ... [49]
Formatiert ... [50]
hat gelöscht: 11
hat formatiert ... [52]
Formatiert ... [51]
hat formatiert ... [53]
Formatiert ... [54]
Formatierte Tabelle ... [55]
hat gelöscht: 21
Formatiert ... [56]
hat formatiert ... [57]
hat gelöscht: Turbulence coefficient ... [58]

Table 3: Model input parameters of the simple and the recharge evaporation model for natural ponds and lakes from the Salar del Huasco. The isotopic composition of inflowing water (δ_{WI}) was inferred from the spring with the most depleted $\delta^{18}O$ value. The isotopic composition of atmospheric vapour (δ_V) was estimated by direct measurement. Evaporation trajectories were modelled with temperature and relative humidity values averaged over 10 (03/19) or 20 days (09/17, 09/18) prior to sampling (Fig. 4), corresponding to the mean seasonal isotopic 'turnover-time' (c.f. Sect. 6.1). Diurnal variations in the evaporation rate were accounted for using daytime (6-18 h) values. The value of the turbulence coefficient was derived from pan evaporation experiment data (cf. Sect. 5.3).

Parameter	2017	2018	2019
$\delta^{18}O_{WI}$ (‰)	-13.28	-13.03	-13.22
d-excess$_{WI}$ (‰)	6.0	5.1	6.2
^{17}O-excess$_{WI}$ (per meg)	15	7	9
$\delta^{18}O_V$ (‰)	-21.0	-21.0	-21.0
d-excess$_V$ (‰)	34	34	34
^{17}O-excess$_V$ (per meg)	23	23	23
Temperature (°C)	7	6	12
Relative humidity (%)	27	23	36
Turbulence coefficient	0.55	0.55	0.55

hat gelöscht: 2
hat formatiert ... [59]
hat gelöscht: For …vaporation trajectories were modelled [60]
hat formatiert ... [61]
Formatiert ... [62]
Formatiert ... [63]
hat formatiert ... [64]
Formatiert ... [65]
hat formatiert ... [66]
Formatiert ... [67]
hat gelöscht: 3
hat formatiert ... [68]
hat formatiert ... [69]
Formatiert ... [70]
Formatiert ... [72]
hat gelöscht: 19.4
hat formatiert ... [73]
hat gelöscht: 19.4
hat formatiert ... [74]
hat gelöscht: 19.4
hat formatiert ... [71]
hat formatiert ... [75]
hat formatiert ... [76]
Formatiert ... [77]
hat gelöscht: 30
hat formatiert ... [78]
hat gelöscht: 30
hat formatiert ... [79]
hat gelöscht: 10
hat formatiert ... [80]
Formatiert ... [82]
hat gelöscht: 18
hat formatiert ... [83]
hat gelöscht: 18
hat formatiert ... [84]
hat gelöscht: 18
hat formatiert ... [81]
hat formatiert ... [85]
hat formatiert ... [86]
Formatiert ... [87]
hat gelöscht: 6
hat formatiert ... [88]
hat gelöscht: 11
hat formatiert ... [89]
hat formatiert ... [90]
Formatiert ... [91]
hat gelöscht: 23
hat formatiert ... [92]
hat gelöscht: 30
hat formatiert ... [93]
hat gelöscht: 44
hat formatiert ... [94]
hat formatiert ... [95]
Formatiert ... [96]

Seite 6: [1] hat gelöscht	Claudia Voigt	19.11.20 17:30:00
Seite 8: [2] hat gelöscht	Claudia Voigt	19.11.20 17:30:00
Seite 8: [3] hat gelöscht	Claudia Voigt	19.11.20 17:30:00
Seite 14: [4] hat gelöscht	Claudia Voigt	19.11.20 17:30:00
Seite 14: [5] hat gelöscht	Claudia Voigt	19.11.20 17:30:00
Seite 14: [6] hat gelöscht	Claudia Voigt	19.11.20 17:30:00
Seite 14: [7] hat gelöscht	Claudia Voigt	19.11.20 17:30:00
Seite 14: [8] hat gelöscht	Claudia Voigt	19.11.20 17:30:00
Seite 14: [9] hat gelöscht	Claudia Voigt	19.11.20 17:30:00
Seite 14: [10] hat gelöscht	Claudia Voigt	19.11.20 17:30:00
Seite 16: [11] hat gelöscht	Claudia Voigt	19.11.20 17:30:00
Seite 16: [12] hat gelöscht	Claudia Voigt	19.11.20 17:30:00
Seite 16: [13] hat gelöscht	Claudia Voigt	19.11.20 17:30:00
Seite 16: [14] hat gelöscht	Claudia Voigt	19.11.20 17:30:00
Seite 19: [15] hat gelöscht	Claudia Voigt	19.11.20 17:30:00

Seite 23: [19] Formatiert **Claudia Voigt** **19.11.20 17:30:00**

Einzug: Links: 0 cm, Hängend: 0.85 cm, Keine Absatzkontrolle, Leerraum zwischen asiatischem und westlichem Text nicht anpassen, Leerraum zwischen asiatischem Text und Zahlen nicht anpassen

Seite 23: [20] Formatiert **Claudia Voigt** **19.11.20 17:30:00**

Keine Absatzkontrolle, Leerraum zwischen asiatischem und westlichem Text nicht anpassen, Leerraum zwischen asiatischem Text und Zahlen nicht anpassen

Seite 27: [21] hat gelöscht **Claudia Voigt** **19.11.20 17:30:00**

Seite 32: [22] hat gelöscht **Claudia Voigt** **19.11.20 17:30:00**

Seite 33: [23] hat gelöscht **Claudia Voigt** **19.11.20 17:30:00**

Seite 33: [23] hat gelöscht **Claudia Voigt** **19.11.20 17:30:00**

Seite 33: [23] hat gelöscht **Claudia Voigt** **19.11.20 17:30:00**

Seite 33: [23] hat gelöscht **Claudia Voigt** **19.11.20 17:30:00**

Seite 33: [23] hat gelöscht **Claudia Voigt** **19.11.20 17:30:00**

Seite 33: [23] hat gelöscht **Claudia Voigt** **19.11.20 17:30:00**

Seite 33: [23] hat gelöscht **Claudia Voigt** **19.11.20 17:30:00**

Seite 33: [23] hat gelöscht **Claudia Voigt** **19.11.20 17:30:00**

Seite 33: [23] hat gelöscht **Claudia Voigt** **19.11.20 17:30:00**

Seite 33: [23] hat gelöscht **Claudia Voigt** **19.11.20 17:30:00**

Seite 33: [23] hat gelöscht **Claudia Voigt** **19.11.20 17:30:00**

Seite 33: [23] hat gelöscht **Claudia Voigt** **19.11.20 17:30:00**

Seite 33: [23] hat gelöscht **Claudia Voigt** **19.11.20 17:30:00**

Seite 33: [23] hat gelöscht **Claudia Voigt** **19.11.20 17:30:00**

Seite 33: [23] hat gelöscht **Claudia Voigt** **19.11.20 17:30:00**

Seite 34: [24] hat gelöscht **Claudia Voigt** **19.11.20 17:30:00**

Seite 34: [25] hat gelöscht **Claudia Voigt** **19.11.20 17:30:00**

Seite 34: [26] hat formatiert **Claudia Voigt** **19.11.20 17:30:00**

Schriftfarbe: Text 1

Seite 34: [27] hat gelöscht **Claudia Voigt** **19.11.20 17:30:00**

Seite 34: [28] hat gelöscht **Claudia Voigt** **19.11.20 17:30:00**

Seite 34: [29] hat formatiert **Claudia Voigt** **19.11.20 17:30:00**

Schriftart: 10 Pt.

Seite 34: [30] Formatiert **Claudia Voigt** **19.11.20 17:30:00**

Zentriert, Zeilenabstand: Mehrere 1.15 ze

Seite 34: [31] hat formatiert **Claudia Voigt** **19.11.20 17:30:00**

Schriftart: 10 Pt.

Seite 34: [32] Formatiert **Claudia Voigt** **19.11.20 17:30:00**

Zentriert, Zeilenabstand: Mehrere 1.15 ze

Seite 34: [33] Formatiert **Claudia Voigt** **19.11.20 17:30:00**

Zeilenabstand: Mehrere 1.15 ze

Seite 34: [34] hat formatiert **Claudia Voigt** **19.11.20 17:30:00**

Schriftart: 10 Pt.

Seite 34: [35] Formatiert **Claudia Voigt** **19.11.20 17:30:00**

Zentriert, Zeilenabstand: Mehrere 1.15 ze

Seite 34: [36] Formatiert **Claudia Voigt** **19.11.20 17:30:00**

Zeilenabstand: Mehrere 1.15 ze

Seite 34: [39] Formatiert **Claudia Voigt** **19.11.20 17:30:00**

Zeilenabstand: Mehrere 1.15 ze

Seite 34: [40] hat formatiert **Claudia Voigt** **19.11.20 17:30:00**

Schriftart: 10 Pt.

Seite 34: [41] Formatiert **Claudia Voigt** **19.11.20 17:30:00**

Zentriert, Zeilenabstand: Mehrere 1.15 ze

Seite 34: [42] Formatiert **Claudia Voigt** **19.11.20 17:30:00**

Zeilenabstand: Mehrere 1.15 ze

Seite 34: [43] hat formatiert **Claudia Voigt** **19.11.20 17:30:00**

Schriftart: 10 Pt.

Seite 34: [44] Formatiert **Claudia Voigt** **19.11.20 17:30:00**

Zentriert, Zeilenabstand: Mehrere 1.15 ze

Seite 34: [45] Formatiert **Claudia Voigt** **19.11.20 17:30:00**

Zeilenabstand: Mehrere 1.15 ze

Seite 34: [46] hat formatiert **Claudia Voigt** **19.11.20 17:30:00**

Schriftart: 10 Pt.

Seite 34: [47] Formatiert **Claudia Voigt** **19.11.20 17:30:00**

Zentriert, Zeilenabstand: Mehrere 1.15 ze

Seite 34: [48] Formatiert **Claudia Voigt** **19.11.20 17:30:00**

Zeilenabstand: Mehrere 1.15 ze

Seite 34: [49] hat formatiert **Claudia Voigt** **19.11.20 17:30:00**

Schriftart: 10 Pt.

Seite 34: [50] Formatiert **Claudia Voigt** **19.11.20 17:30:00**

Zentriert, Zeilenabstand: Mehrere 1.15 ze

Seite 34: [51] Formatiert **Claudia Voigt** **19.11.20 17:30:00**

Zeilenabstand: Mehrere 1.15 ze

Seite 34: [52] hat formatiert **Claudia Voigt** **19.11.20 17:30:00**

Schriftart: 10 Pt.

Seite 34: [53] hat formatiert **Claudia Voigt** **19.11.20 17:30:00**

Schriftart: 10 Pt.

Seite 34: [54] Formatiert **Claudia Voigt** **19.11.20 17:30:00**

Zentriert, Zeilenabstand: Mehrere 1.15 ze

Seite 34: [57] hat formatiert **Claudia Voigt** **19.11.20 17:30:00**

Schriftart: 10 Pt.

Seite 34: [58] hat gelöscht **Claudia Voigt** **19.11.20 17:30:00**

Seite 35: [59] hat formatiert **Claudia Voigt** **19.11.20 17:30:00**

Schriftart: Kursiv

Seite 35: [59] hat formatiert **Claudia Voigt** **19.11.20 17:30:00**

Schriftart: Kursiv

Seite 35: [60] hat gelöscht **Claudia Voigt** **19.11.20 17:30:00**

Seite 35: [60] hat gelöscht **Claudia Voigt** **19.11.20 17:30:00**

Seite 35: [60] hat gelöscht **Claudia Voigt** **19.11.20 17:30:00**

Seite 35: [60] hat gelöscht **Claudia Voigt** **19.11.20 17:30:00**

Seite 35: [60] hat gelöscht **Claudia Voigt** **19.11.20 17:30:00**

Seite 35: [61] hat formatiert **Claudia Voigt** **19.11.20 17:30:00**

Schriftart: 10 Pt.

Seite 35: [62] Formatiert **Claudia Voigt** **19.11.20 17:30:00**

Zeilenabstand: Mehrere 1.15 ze

Seite 35: [63] Formatiert **Claudia Voigt** **19.11.20 17:30:00**

Zentriert, Zeilenabstand: Mehrere 1.15 ze

Seite 35: [64] hat formatiert **Claudia Voigt** **19.11.20 17:30:00**

Schriftart: 10 Pt.

Seite 35: [65] Formatiert **Claudia Voigt** **19.11.20 17:30:00**

Zeilenabstand: Mehrere 1.15 ze

Seite 35: [66] hat formatiert **Claudia Voigt** **19.11.20 17:30:00**

Schriftart: 10 Pt.

Seite 35: [67] Formatiert **Claudia Voigt** **19.11.20 17:30:00**

Zeilenabstand: Mehrere 1.15 ze

Seite 35: [70] Formatiert **Claudia Voigt** **19.11.20 17:30:00**

Zeilenabstand: Mehrere 1.15 ze

Seite 35: [71] hat formatiert **Claudia Voigt** **19.11.20 17:30:00**

Schriftart: 10 Pt.

Seite 35: [72] Formatiert **Claudia Voigt** **19.11.20 17:30:00**

Zeilenabstand: Mehrere 1.15 ze

Seite 35: [73] hat formatiert **Claudia Voigt** **19.11.20 17:30:00**

Schriftart: 10 Pt.

Seite 35: [74] hat formatiert **Claudia Voigt** **19.11.20 17:30:00**

Schriftart: 10 Pt.

Seite 35: [75] hat formatiert **Claudia Voigt** **19.11.20 17:30:00**

Schriftart: 10 Pt.

Seite 35: [76] hat formatiert **Claudia Voigt** **19.11.20 17:30:00**

Schriftart: 10 Pt.

Seite 35: [77] Formatiert **Claudia Voigt** **19.11.20 17:30:00**

Zeilenabstand: Mehrere 1.15 ze

Seite 35: [78] hat formatiert **Claudia Voigt** **19.11.20 17:30:00**

Schriftart: 10 Pt.

Seite 35: [79] hat formatiert **Claudia Voigt** **19.11.20 17:30:00**

Schriftart: 10 Pt.

Seite 35: [80] hat formatiert **Claudia Voigt** **19.11.20 17:30:00**

Schriftart: 10 Pt.

Seite 35: [81] hat formatiert **Claudia Voigt** **19.11.20 17:30:00**

Schriftart: 10 Pt.

Seite 35: [82] Formatiert **Claudia Voigt** **19.11.20 17:30:00**

Zeilenabstand: Mehrere 1.15 ze

Seite 35: [83] hat formatiert **Claudia Voigt** **19.11.20 17:30:00**

Schriftart: 10 Pt.

Seite 35: [84] hat formatiert **Claudia Voigt** **19.11.20 17:30:00**

Schriftart: 10 Pt.

Seite 35: [85] hat formatiert **Claudia Voigt** **19.11.20 17:30:00**

Schriftart: 10 Pt.

Seite 35: [88] hat formatiert	Claudia Voigt	19.11.20 17:30:00

Schriftart: 10 Pt.

Seite 35: [89] hat formatiert	Claudia Voigt	19.11.20 17:30:00

Schriftart: 10 Pt.

Seite 35: [90] hat formatiert	Claudia Voigt	19.11.20 17:30:00

Schriftart: 10 Pt.

Seite 35: [91] Formatiert	Claudia Voigt	19.11.20 17:30:00

Zeilenabstand: Mehrere 1.15 ze

Seite 35: [92] hat formatiert	Claudia Voigt	19.11.20 17:30:00

Schriftart: 10 Pt.

Seite 35: [93] hat formatiert	Claudia Voigt	19.11.20 17:30:00

Schriftart: 10 Pt.

Seite 35: [94] hat formatiert	Claudia Voigt	19.11.20 17:30:00

Schriftart: 10 Pt.

Seite 35: [95] hat formatiert	Claudia Voigt	19.11.20 17:30:00

Schriftart: 10 Pt.

Seite 35: [96] Formatiert	Claudia Voigt	19.11.20 17:30:00

Zeilenabstand: Mehrere 1.15 ze

Seite 35: [97] hat formatiert	Claudia Voigt	19.11.20 17:30:00

Schriftart: 10 Pt.

Seite 35: [98] hat formatiert	Claudia Voigt	19.11.20 17:30:00

Schriftart: 10 Pt.

Seite 35: [99] hat formatiert	Claudia Voigt	19.11.20 17:30:00

Schriftart: 10 Pt.